Glucose-6-Phosphate Dehydrogenase from the Human Pathogen Trypanosoma cruzi Evolved Unique Structural Features to Support Efficient Product Formation

Cecilia Ortíz, Horacio Botti, Alejandro Buschiazzo, Marcelo Comini

Glucose-6-phosphate dehydrogenase from the human pathogen *Trypanosoma cruzi* evolved unique structural features to support efficient product formation.

Cecilia Ortíz[1], Horacio Botti[2,*], Alejandro Buschiazzo[2,3,#], Marcelo A. Comini[1,#]

[1] Laboratory Redox Biology of Trypanosomes and [2] Laboratory of Molecular & Structural Microbiology, Institut Pasteur de Montevideo, Mataojo 2020, 11400-Montevideo, Uruguay. [3] Department of Microbiology, Institut Pasteur, rue du Dr Roux 75015, Paris, France.

* Current affiliation: Laboratory of Integrative Biophysics, Departamento de Biofísica, Facultad de Medicina, Universidad de la República, Montevideo, Uruguay.

Running title: *Trypanosoma cruzi* G6PDH

 # Corresponding author(s):

Dr. Marcelo A. Comini, Laboratory Redox Biology of Trypanosomes, Institut Pasteur de Montevideo, 11400-Montevideo, Uruguay. Telephone: 00598-25220910 extension 164; FAX: 00598-2522 4185; E-mail: mcomini@pasteur.edu.uy

Dr. Alejandro Buschiazzo, Laboratory of Molecular & Structural Microbiology, Institut Pasteur de Montevideo, Mataojo 2020, 11400-Montevideo, Uruguay. Telephone: 00598-25220910; FAX: 00598-2522 4185; E-mail: alebus@pasteur.edu.uy

ABSTRACT

Glucose-6-phosphate dehydrogenase (G6PDH) is the key enzyme supplying reducing power (NADPH) to the cells, by oxidation of glucose-6-phosphate (G6P), and in the process providing a precursor of ribose-5-phosphate. G6PDH is also a virulence factor of pathogenic trypanosomatid parasites. To uncover the biochemical and structural features that distinguish *Tc*G6PDH from its human homologue, we have now solved the crystal structures of the G6PDH from *Trypanosoma cruzi* (*Tc*G6PDH), alone and in complex with G6P. *Tc*G6PDH crystallized as a tetramer, and enzymatic assays further indicated that the tetramer is the active form in the parasite, in contrast to human G6PDH, which displays higher activity as a dimer. This quaternary structure was shown to be particularly stable. The molecular reasons behind this disparity were unveiled by structural analyses: a *Tc*G6PDH-specific residue, R323, is located at the dimer-dimer interface, critically contributing with two salt bridges per subunit that are absent in the human enzyme. This explains why *Tc*G6PDH dimerization impaired enzyme activity. The parasite protein is also distinct in displaying a 37 amino acids extension at the N-terminus, which comprises the non-conserved C8 and C34 involved in the covalent linkage of two neighboring protomers. In addition, a cysteine triad (C53, C94 and C135) specific of Kinetoplastid G6PDHs proved critical for stabilization of *Tc*G6PDH active site. Based on the structural and biochemical data, we posit that the N-terminal region and the catalytic site are highly dynamic. The unique structural features of *Tc*G6PDH pave the way toward the design of efficacious and highly specific anti-trypanosomal drugs.

KEYWORDS: NADP, pentose phosphate, virulence, disulfide bridge, allosteric, Chagas disease

ABBREVIATIONS

ASU, asymmetric unit; DTT, dithiotreitol; G6P, glucose 6-phosphate; G6PDH, glucose 6-phosphate dehydrogenase; *Hs*G6PDH, *Homo sapiens* glucose 6-phosphate dehydrogenase; Δ37N, deletion mutant lacking the first 37 N-terminal residues; Δ57N, deletion mutant lacking the first 57 N-terminal residues; PPP, pentose phosphate pathway; rmsd, root mean squared deviation; SDS-PAGE, sodium dodecyl sulphate-polyacrylamide gel electrophoresis; SEC, size exclusion chromatography; *T.* cruzi, *Trypanosoma cruzi*; *Tc*, *Trypanosoma cruzi*.

INTRODUCTION

The diseases caused by several species of the genera *Trypanosoma* and *Leishmania* are among the most prevalent and devastating zoonotic infections in tropical and subtropical regions of the world. In the Americas, *Trypanosoma cruzi* is responsible for Chagas´ disease, typically evolving into a highly disabling chronic form that compromises vital organs (e.g. heart, digestive tract). The infective form of this parasite (trypomastigote) must withstand the action of harmful reactive oxygen and nitrogen species produced by the mammalian host's immune system. Within the host, the parasite invades many different cell types, differentiating into the proliferative intracellular amastigote form. Protection against host-borne radicals and oxidants, as well as the parasites' proliferation, both require for the supply of reducing power in the form of NADPH [1,2]. To fulfill this demand, the pathogen expresses several $NADP^+$-linked dehydrogenases that are developmentally regulated [3-7]. Among them, glucose-6-phosphate dehydrogenase (G6PDH) plays a housekeeping role in the generation of NADPH in trypanosomes [4,8]. G6PDH catalyzes a two-electron oxidation of G6P and reduction of $NADP^+$, producing 6-phosphogluconolactone (6PGL), NADPH and H^+ [9]

$$NADP^+ + G6P \rightleftharpoons 6PGL + NADPH + H^+ \qquad \Delta G^{\circ\prime} = -2.3 \pm 2.6 \text{ kJ/mol} \qquad (1)$$

G6PDH is the first enzyme from the oxidative branch of the pentose phosphate pathway (PPP), a pathway that also provides essential nucleotide precursors and phosphorylated sugar intermediates [10,11]. The PPP has been shown to be operative in epimastigotes of *T. cruzi* [4,12] and all the enzymes of the pathway are present in the four major developmental stages of the parasite [12]. Higher glucose consumption *via* the PPP and increased levels of G6PDH, have been associated with higher virulence and parasite infectivity [4,12-16]. In fact, the content of G6PDH is higher in the clinically relevant stages of *T. cruzi,* and its enzymatic activity increased upon oxidative insult [14]. G6PDH has been shown to be essential for *in vitro* survival of *T. brucei* [8] and to confer *Leishmania* increased protection towards reactive

oxygen species [16] and resistance against several drugs in clinical use [17]. Overall, these are overwhelming pieces of evidence pinpointing G6PDH as an attractive anti-trypanosomatid drug target [18,19].

G6PDH from different Trypanosomatid species share similar kinetic constants [14,20-22], indicating a conserved core of catalytic and ligand-binding amino acid residues. Interestingly, the *T. cruzi* enzyme (*Tc*G6PDH) is inhibited by its product NADPH, and also inactivated by reducing agents [14], but the mechanism of this redox-based regulation is still unknown. A truncated form of *Tc*G6PDH, lacking the first 37 amino acids (Δ37N-*Tc*G6PDH) had previously been crystallized by our group [23].

We have now determined the crystal structures of free *Tc*G6PDH (PDB ID 6D23), as well as bound to the substrate glucose-6-phosphate (G6P) (PDB 6D24). *Tc*G6PDH displayed a tetrameric architecture, in contrast with previous reports [14], that claimed *Tc*G6PDH to be a dimer as most G6PDH homologues from different species [24-28]. More recently, the crystal structure of a shorter deletion mutant (Δ57N-*Tc*G6PDH) in complex with G6P and NADPH was also reported [29].

We now performed an in-depth comparative analysis between *Tc*G6PDH and the human counterpart, providing with structural and functional evidence of unique, parasite-specific, molecular features. Integrating our crystallographic, enzymatic and mutagenesis data, we propose a new model for the structural role of charged residues located in the dimer-dimer interface and for the redox-dependent allosteric regulation of *Tc*G6PDH by N-terminal cysteines, and establish a rational framework for the design of drug candidates targeting this enzyme.

RESULTS and DISCUSSION

Crystal structure of Δ37N-*Tc*G6PDH

A construct of *Tc*G6PDH expressing a protein that lacks the first 37 amino acids towards the N-terminus (Δ37N-*Tc*G6PDH), resulted in crystals that diffracted X-rays substantially better than the full-length form (*Tc*G6PDH$_L$), allowing for the 3D structure of Δ37N-*Tc*G6PDH

to be solved. We had previously reported on the crystallization conditions of Δ37N-*Tc*G6PDH [23], both free and in complex with glucose-6-phosphate (G6P). Both crystal structures were now determined by X-ray diffraction, and refined to 2.85 Å (PDB 6D23) and 3.35 Å (PDB 6D24) resolution, respectively (Table 1). Both corresponded to the same monoclinic crystal form, with four molecules in the ASU (Fig. 1A), and G6P clearly visible in electron density for the complexed variant. *Tc*G6PDH is a tetramer, which can be well described as a dimer of dimers, with each dimer burying a significantly larger solvent-exposed surface between protomers, than that between dimers: the intra-dimeric interface (~5500 $Å^2$) engages ~10.5% of the surface of each separate protomer, whereas the smaller inter-dimeric area (~4000 $Å^2$) corresponds to ~4% of each dimer's surface. Both dimers are positioned in a back-to-back orientation forming the tetramer. After we released these structures in the PDB, a tetragonal crystal structure of *Tc*G6PDH was reported (PDB 5AQ1) [29], corresponding to a shorter truncated form lacking the first 57 N-terminal residues. Beside the distinct crystal packings, our structures share identical tetrameric architecture as the tetragonal form, with slight differences in terms of inter-dimer symmetry: the tetragonal form displays only three protomers per ASU.

The point group symmetry of the Δ37N-*Tc*G6PDH tetramer is 222, identical to that of the human enzyme (*Hs*G6PDH, PDB 1QKI) [30]. The crossing angle of the two major dimer axes (i.e. axes that connect the centroids of the two protomers in each dimer) is ~40º in Δ37N-*Tc*G6PDH (Fig 1B) compared to ~30º in *Hs*G6PDH, unveiling a substantial orientation rearrangement of the dimer of dimers organization. Superimposing separately each dimer of both enzymes also reveals an approximate 20º rotation of one protomer with respect to the other in both dimers, whereas the intra-protomer variations superimposing 473 Cα positions are all very similar, with pair-wise figures of 1.8-1.9 Å rmsd. Thus, the tetramerization of the trypanosomal protein does not entail substantial structural changes at the subunit level. The *Tc*G6PDH inter-protomer buried surface engages extensive hydrophobic and electrostatic contacts between subunits. The inter-dimer interface displays slightly larger contributions from

the crossing protomers (~500 Å^2) compared to the two pair of monomers on the same side (~370 Å^2). The interdimer interface is stabilized mainly by polar contacts (8 salt bridges and 9 hydrogen bonds). It is worth highlighting that *Hs*G6PDH reveals similar inter-protomer interfaces stabilizing each dimer, but a very different inter-dimer surface, smaller (~1200 Å^2) than that of *Tc*G6PDH, and with more limited interactions between crossed (~350 Å^2) and side-by-side (~270 Å^2) protomers.

*Tc*G6PDH displays the expected tertiary structure of G6PDHs (Fig. 1C), which has been described before [29], comprising an N-terminal coenzyme-binding domain (residues 1–246) and a C-terminal domain involved in subunit dimerization (residues 251–555; Fig. 2). The two domains are connected by a one-turn 3_{10}-helix (residues 247-249). The electron density corresponding to residues 38–51, is not visible in any of the subunits on the two crystal structures, suggesting that this region is highly flexible. Comparison of the free form of Δ37N-*Tc*G6PDH to the one complexed with the G6P substrate, reveals insignificant overall differences, with ~0.8 Å rmsd in all 332 Cα positions within secondary structure elements. Only minor local shifts are observed in solvent-exposed loops.

*Tc*G6PDH$_L$ forms highly stable tetramers in solution

Human G6PDH exhibits a dynamic equilibrium between an enzymatically inactive monomeric species, with active dimeric and tetrameric forms (the dimer being the predominant arrangement), an equilibrium that is influenced by the environment's physicochemical properties and presence of ligands [31]. For instance, NADP$^+$ and G6P stabilize, respectively, the dimeric and monomeric forms of *Hs*G6PDH [32,33]. In contrast, the oligomeric state adopted by the active form of *Tc*G6PDH is still a matter of debate, with evidence favoring a dimeric organization [14] contrasting with reports of *Tc*G6PDH forming stable tetramers in physiological buffer solutions and in crystals [23,29]. To further explore about the relevant quaternary structure of the trypanosomatid enzyme, *Tc*G6PDH$_L$ was subjected to SEC in the presence of saturating substrate concentrations (NADP$^+$ or G6P; see the kinetic parameters in Table 2). The SEC profiles of *Tc*G6PDH$_L$ did not change significantly in the presence or

absence of ligands (Fig. 3A), always displaying a very stable tetrameric configuration. Dehydroepiandrosterone, a G6PDH inhibitor [22], was also assayed, revealing no detectable alteration of *Tc*G6PDH$_L$'s SEC migration. Beside the action of specific ligands or substrates, it is known that *Hs*G6PDH dimers are stabilized by increasing ionic strength or removal of Mg^{++} [32]. Again contrasting the human enzyme's properties, *Tc*G6PDH$_L$ tetramers were refractory to high ionic strength or to the absence of Mg^{++} (Fig. 3B). Covalent interactions stabilizing the tetrameric organization of the trypanosomal G6PDH were also ruled out, given that no species of low molecular mass were detected under reducing conditions (Fig. 3B).

In sum, *Tc*G6PDH$_L$ forms highly stable tetramers associated through non-covalent interactions, in contrast to the human enzyme's properties (Fig. S2).

*Tc*G6PDH R323 is a key determinant of tetramerization

The dimer-dimer interface of *Tc*G6PDH reveals eight ionic bonds (Fig. 4A): R323-D332', AR323-E333', R265-D390', K321-D390', D390-R265', D390-K321', D332-R323' and E333-R323' (the prime symbol identifies residues within the neighboring dimer, chain A of dimer 1 interfaces with chain C in dimer 2, and the same range of interactions can be identified between dimer 2's chain B, and dimer 1's chain D). Although similarly charged residues occupy equivalent positions in *Hs*G6PDH (Fig. 2), only four of them are engaged in forming salt bridges: K275-E347´ (K321-D390' in *Tc*G6PDH) and E287-K290´ (E333-Q336' *Tc*G6PDH; note that the salt bridge is absent in the latter case, since K290 is substituted by Q336 in the trypanosomal enzyme). Moreover, a comparison of the tetrameric configurations of these proteins reveals that, due to the shift in relative orientations, the pair R219-E347' of *Hs*G6PDH is separated by 7 Å whereas the side chain groups of the equivalent residues in *Tc*G6PDH (R265-D390') are only 2.8 Å apart, and hence, at a suitable distance for ionic interaction. More importantly, the substitution of R323 by an alanine (A277) eliminates all at once four salt bridges in the human enzyme. R323 in *Tc*G6PDH is located within a loop connecting helices α13 and α14, interacting with both D332 and E333 in helix α14 from the neighboring dimer. As a means to verify the relevance of the ionic bonds in holding the dimers

together within the tetramer, *Tc*G6PDH$_L$ was resolved by SEC at lower pH (5.5). Under such condition, the major species eluted with a lower apparent molecular mass compared to the same sample analyzed at pH 7.5 (Fig. 4B), strongly suggesting partial dissociation of the tetramer. We next replaced R323 by a glycine using genetic engineering, and the point-mutated protein (*Tc*G6PDH$_L$-R323G) now behaved as a pure dimeric species in SEC (Fig 4B). Such elution pattern did not change under reducing conditions, further supporting that covalent interactions do not contribute to the dimeric assemble of the protein.

A positively charged residue at position 323 is strictly conserved in all G6PDH enzymes from Kinetoplastid protozoa (with Arg largely prevailing over Lys) with the sole exceptions of the non-pathogenic *Leishmania enrietti*, *Crithidia fasciculata* and *Leptomonas* spp., which possess a Gln/Asn/Ser (Fig. S1). Moreover, the pair D332/E333 is equally conserved. The absence of a positively charged residue occupying position 323 in orthologues from other lineages (Fig. 2), suggests that these proteins will not form stable tetramers. In order to verify this hypothesis, recombinant G6PDH from *C. fasciculata* (*Cf*G6PDH$_L$), which presents an asparagine residue (N325) substituting the otherwise conserved R323 of *Tc*G6PDH, was subjected to SEC. Under reducing (5 mM DTT) conditions and 0.5 M NaCl, *Cf*G6PDH$_L$ eluted with an apparent molecular weight of ~260 kDa, consistent with the protein being a tetramer (the sequence-derived molecular weight of the His-tagged *Cf*G6PDH$_L$ monomer is 65 kDa). At a higher ionic strength (1 M NaCl), most of *Cf*G6PDH$_L$ still eluted as a tetrameric species, with a minor peak corresponding to the monomer (68 kDa apparent molecular weight). At pH 6.5, which is one unit higher than that required to dimerize *Tc*G6PDH$_L$ (pH 5.5; Fig. 4B), *Cf*G6PDH$_L$ eluted as a broad peak, with a maximum corresponding to the dimer (~118 kDa) (Fig. 5A). This behavior is consistent with the hypothesis described above, indicating that fewer or weaker electrostatic interactions are stabilizing the dimer-dimer interaction in *Cf*G6PDH$_L$, compared to *Tc*G6PDH. However, in contrast to *Hs*G6PDH that also lacks R323 and is predominantly dimeric (Fig. S2), *Cf*G6PDH$_L$ proved to be tetrameric, suggesting that residues other than R323 might contribute to stabilize the quaternary structure of the protein. Structural analysis of *Cf*G6PDH$_L$ (using a homology-based model generated with *Tc*G6PDH

PDB 6D24 as the template), anticipates R331 (close to N325) to be well located to establish a salt bridge with D334 (equivalent to *Tc*G6PDH D332) from a neighboring dimer (Fig. 5B). We speculate that this R331-D334´ salt bridge in *Cf*G6PDH$_L$ may partially compensate for the stabilizing effect of the two salt bridges R323-D332´ and R323-E333´ in *Tc*G6PDH$_L$ (Fig. 5C). Taken together, our data lead us to posit that all Kinetoplastids bearing the R323-D332/E333 salt bridges will likely form stable tetramers.

Structural role of R323 in *Tc*G6PDH enzymatic activity

Compared to wild-type *Tc*G6PDH$_L$ (99 U/mg), the specific activity of the dimeric R323G mutant (32 U/mg) was 68% lower, indicating that quaternary structure alteration impairs enzymatic activity. Kinetic characterization of the R323G mutant revealed a 4- and 7-fold increase in K_m^{app} for $NADP^+$ and G6P, respectively, compared to the wild-type enzyme (Table 2). Furthermore, the point-mutant displayed 85- and 41-fold lower apparent catalytic efficiencies for G6P and $NADP^+$, respectively (Table 2), indicating that the dimer also catalyzes the enzymatic reaction slower. Therefore, R323 appears to be allosterically connected to the active site.

An allosteric binding site for $NADP^+$ toward the C-terminal portion of *Hs*G6PDH dimerization domain has been reported to stabilize its active, dimeric form [30,34]. In fact, *Hs*G6PDH mutants such as R393G or R393H, isolated from clinical cases and displaying impaired binding of allosteric $NADP^+$, are remarkably unstable and show 2.5- to 13-fold increase of the K_m^{G6P} (and a minor 1.3-fold increase of K_m^{NADP+}) when compared to the wild-type enzyme [33,36]. The protein main-chain trace, as well as several key NADP-binding residues, are conserved between the human and *T. cruzi* enzymes in this region [29]. However, *Tc*G6PDH displays substitutions in three positions among the critical amino acids that bind the adenosine moiety: Y503, K366 and R487 in *Hs*G6PDH [35] are replaced respectively by T544, L409 and C528 in *Tc*G6PDH (Fig. 6A). This raises the question as to whether structural NADP+ may bind and stabilize dimeric *Tc*G6PDH in a catalytically competent conformation. To address this point, the structural $NADP^+$-binding site of *Hs*G6PDH

was partially reconstituted in the *Tc*G6PDH$_L$ R323G mutant by substituting C528 for an arginine (C528R). There is a second reason for choosing this site to mutate, besides the fact that the basic residue R487 (occupied by C528 in *Tc*G6PDH), is critical for non-catalytic NADP$^+$-binding in the human enzyme [30,35] (Fig. 2). In *Tc*G6PDH$_L$, C528 is forming an intramolecular disulfide with C552 (chains A and B) or harbors a negative charge due to oxidation of its sulfur atom to a sulfenic acid (chains C and D) (Fig. 6A), according to crystallographic data for Δ37N-*Tc*G6PDH in complex with G6P. In consequence, binding of structural NADP$^+$ to this site in *Tc*G6PDH would be impaired by steric or electrostatic effects. Interestingly, the *Tc*G6PDH$_L$ double mutant R323G-C528R displayed K_m^{app} figures for NADP$^+$ and G6P that are very similar to those of the wild-type enzyme, and k_{cat} values as low as those of the single R323G mutant (Table 2). Altogether, this strongly suggests that partial reconstruction of the structural site for NADP$^+$ in dimeric *Tc*G6PDH$_L$ restores substrates´ binding, but not the active conformation of the enzyme.

Detailed inspection of the *Tc*G6PDH structure provides with clues on the structural role of R323 in the conformation of the enzyme´s active site. R323 is located within a loop that is contiguous to structural elements (from E285 to R323) engaged in G6P-binding (e.g. E285 and D304) and catalysis (H309) (Fig. 2 and 5B; see Table 2). The packing effect of the inter-dimer salt bridges between R323 and D332/E333, stabilizes the R323-containing loop and the preceding structural elements that are part of the active site (β7-α12 loop and helices α12 and α13). In the R323G mutant such a stabilizing effect is lost, leading to lower K_m^{app} values and a catalytically non-competent conformation of the active site.

In sum, our results support the notion of a bidirectional coupling between the active site and the tetramerization surface in *Tc*G6PDH, and that the tetrameric structure of *Tc*G6PDH surrogates the active site-stabilizing role of the second, non-catalytic NADP$^+$-binding site, otherwise naturally present in dimeric G6PDHs.

Cysteine 8 and 34 within the N-terminal extension of *Tc*G6PDH form intra-dimer disulfide bridges

Prior work has shown that recombinant and native *Tc*G6PDH$_L$ were inactivated by treatment with mM concentrations of DTT and/or GSH, while Δ37N-*Tc*G6PDH was unaffected by such reducing agents [14]. This suggests that cysteine residues within the N-terminal extension of *Tc*G6PDH$_L$ might be forming a covalent bond(s) modulating enzymatic activity. As a first approach to elucidate whether the posited disulfide bond(s) is intra- or inter-molecular, different versions of *Tc*G6PDH were subjected to SDS-PAGE in the presence or absence of a reducing agent (Fig. 7A). Interestingly, under reducing conditions, *Tc*G6PDH$_L$ migrated as a single ~60 kDa species, whereas a heterogeneous population was revealed under non-reducing conditions, with a major form of ~120 kDa that corresponds to a dimer. In contrast, Δ37N-*Tc*G6PDH showed always a single ~55 kDa form (monomeric), independent of its oxidation state, indicating that C8 and/or C34 establish inter-monomer disulfide bonds. The elution of *Tc*G6PDH$_L$-R323G as a dimer in SEC under non-reducing conditions (Fig. 3B), was indicative that the covalent bond is intra- and not inter-dimeric. Comforting this observation, under non-reducing SDS-PAGE, this mutant showed a similar migration profile as that of *Tc*G6PDH$_L$, in particular with the appearance of a band corresponding to a dimer (~120 kDa; Fig. 7A).

Next, we investigated which cysteines from the N-terminal extension participate in the formation of the covalent link between subunits of the dimer. Single (C8S and C34S) and double (C8S/C34S) *Tc*G6PDH$_L$ mutants were produced and stored for one week in the absence of reducing agents (time-point based on preliminary spontaneous oxidation observations), prior to Western blot analyses. For each mutant the following samples were prepared, separated in a non-reducing SDS-PAGE and immunoblotted with anti-*Tc*G6PDH serum: i) untreated protein (spontaneous oxidation), ii) protein reduced with a 60-fold molar excess of DTT and iii), upon removal of excess reducing agent, oxidized with a 60-fold molar excess of glutathione disulfide (GSSG) for 45 min. For all Cys mutants treated with DTT the polyclonal anti-serum recognized a single species of ~60 kDa, which corresponds to the molecular weight of the *Tc*G6PDH$_L$ monomer (Fig. 7B). The monomer was also identified in

the untreated samples of all Cys mutants. However, forms migrating as the dimer (~120 kDa) were also detected in the untreated C8S and C34S mutants, and not in the double C8/34S mutant. This indicates that both C8 and C34 participate in the formation of disulphide bridges between the subunits of each dimer (C8-C8´ and C34-C34´). For all *Tc*G6PDH$_L$ Cys mutants, treatment with GSSG induced almost a full conversion of the monomeric species into large molecular weight covalent multimers without formation of dimers as intermediate species. In conclusion, the assay shows that storage of the sample in the absence of a reducing agent produces a selective oxidation of the N-terminal cysteines whereas GSSG triggers a non-specific oxidation of cysteines residues in *Tc*G6PDH$_L$. Overall, the formation of intra-dimeric disulphide bonds seems to be a fine-tuned redox process.

Although the thiol group(s) from the second subunit that is partnering with C8 and/or C34 remains unknown, structural analysis of *Tc*G6PDH provides some hints. *Tc*G6PDH$_L$ harbors 11 cysteine residues (four more than *Hs*G6PDH) among which only C244 occupies a shared position with the human protein (Fig. 2). In the crystal structure of Δ37N-*Tc*G6PDH, nine cysteines are observed, some of which are engaged in intramolecular disulfides (C53-C135 for PDB 6D23 and C528-C552 for PDB 6D23 and chain A and B of PDB 6D24), others are seen to be oxidized to sulfenic acid (C528 in chain C and D of PDB 6D24; Fig. 5A), buried and inaccessible to the solvent (C195, C278, C377), or located at distances incompatible to establish disulfide bonds with C8 and/or C34 (C195, C278, C349 and C377). Together with the redox Western blot data, structural constraints support the hypothesis that C8 and C34 form intra-dimer disulphide bridges.

The N-terminal extension and cysteines therein, modulate *Tc*G6PDH activity

Previous studies proposed a regulatory role of the N-terminal cysteines in the activity of *Tc*G6PDH [14], based on the sensitivity of *Tc*G6PDH$_L$ but not of Δ37N-TcG6PDH to inhibition by DTT and GSH. However, the molecular mechanism of such regulation remained unknown, and are now partially uncovered by kinetic analysis. First, we compared the kinetic parameters for *Tc*G6PDH$_L$ determined under reducing (WT + DTT) and non-reducing conditions (WT).

Partial reduction of DTT-accessible disulfide bonds, impairs mainly the K_m^{app} for G6P (4-fold increase) and, to a minor extent, for $NADP^+$ (2.4-fold), while increasing the k_{cat}^{app} by ~1.7-fold (see further comments in the next section). Despite this apparent compensation, reduced *Tc*G6PDH$_L$ displays an apparent catalytic efficiency (k_{cat}^{app}/K_m^{app}) for both substrates at least 50% lower than that exhibited by the oxidized enzyme. A potential contribution of the C528-C552 disulfide bond to the kinetic behavior of reduced *Tc*G6PDH$_L$ can be ruled out, because the C528R mutant presented similar K_m^{app} and k_{cat}^{app} values than the WT + DTT sample (Table 2). The kinetic results obtained for WT + DTT should thus be interpreted as an overall contribution of cysteines 8, 34, 53, 94 and 135 to the activity of reduced *Tc*G6PDH$_L$.

Further analysis of the C8/34S *Tc*G6PDH$_L$ double mutant allowed to evaluate the contribution of the intermolecular disulfide to enzyme activity. Compared to the WT enzyme assayed under non-reducing conditions, the mutant presented 5-fold higher K_m^{app} for $NADP^+$ than the WT and a 3-fold lower apparent k_{cat}/K_m for this substrate. Interestingly, C8/34S displayed on the other hand nearly identical kinetic parameters for G6P compared with the WT's (Table 2). In agreement with this behavior, the single C8S and C34S mutants displayed ≥2-fold higher K_m^{app} and k_{cat}^{app}/K_m^{app} values for $NADP^+$. More puzzling was the role of the individual cysteines with regards to G6P. While C8/34S and WT showed no significant difference in K_m^{app}, C8S and C34S showed respectively 4.3- and 2.4-fold higher K_m^{app} for G6P, which translated into lower catalytic efficiencies than the WT or C8/34S (Table 2). Worth noting, nearly half of C8S and C34S *Tc*G6PDH$_L$ are forming inter-dimer disulfide bridges, according to Western blot analyses of non-reduced samples (Fig. 7B). Thus, the kinetic parameters obtained for these single mutants represent an average estimation for redox-heterogeneous samples, suggesting that the real impact of lacking the individual Cys residues is underestimated. On the other hand, assayed under non-reducing conditions and compared to the WT enzyme, the mutant devoid of the N-terminal extension (Δ37N) presented a 3.6-fold higher K_m^{app} for G6P, similar K_m^{app} for $NADP^+$ and a 2-fold increased apparent k_{cat} (Table 2). This indicates that the N-terminal extension plays a role in sculpting the G6P-binding site.

Based on the kinetic analysis we can conclude that the formation of interdimer disulfide bonds mediated by C8 and C34 (and intramolecular disulfides by the C53, C94 and C135 triad) favor enzymatic activity. In contrast, the formation of single inter-dimeric homo-disulfides is detrimental for G6P binding, in particular when the most N-terminal C8 is not involved in the covalent bond. Because this effect is not observed in the absence of both cysteines (C8/34S mutant), it will be interesting to probe in future studies whether the dimeric forms of C8S and C34S represent intermediate species with a not properly folded N-terminal extension impairing, in such a state, G6P binding.

The kinetoplastid-conserved cysteine triad C53, C94 and C135 has a major structural role in sculpting the NADP$^+$-binding and catalytic site in *Tc*G6PDH

*Tc*G6PDH C53, C94 and C135 are highly conserved among Kinetoplastid G6PDHs (Fig. 2 and Fig. S1). According to the structure of Δ37N-*Tc*G6PDH, the thiol groups of this triad are separated 2 to 9 Å from one another, with the pair C53-C135 forming a disulfide bond and C94 buried, likely hydrogen-bonded to H136. Supporting the spatial proximity and redox reactivity of these Cys residues, the structure of Δ57N-*Tc*G6PDH [29] shows a disulfide bridge bonding C94 to C135 (Fig. 8). Although the kinetic analyses presented in previous sections suggest that this Cys triad may contribute to modulating enzyme activity, information about their precise role and significance is still lacking. To gain further insight into these aspects, single Cys-to-Ser *Tc*G6PDH$_L$ mutants (C53S, C94S and C135S) were generated and their kinetic constants determined under non-reducing conditions (Table 2).

Compared to the WT enzyme, all kinetic parameters were negatively affected in the three points mutants. For instance, the K_m^{app} for NADP$^+$ shows a ≥21-fold increase for all three mutants, and the K_m^{app} for G6P is 20-, 2- and 9-fold higher for C53S, C94S and C135S, respectively. The apparent k_{cat} values for both substrates dropped between 21 to 56 times for C53S and C94S. Always comparing to WT, the C53S and C94S mutants displayed strikingly lower k_{cat}^{app}/K_m^{app} for both substrates (130- to 955-fold). For C135S, the unchanged (for G6P) or 1.8-fold increased (for NADP$^+$) k_{cat}^{app}, partially mitigated the final effect in kinetic efficiency

for both substrates (respectively 8.5- and 21-fold lower for G6P and $NADP^+$). Both K_m^{app} and k_{cat}^{app}/K_m^{app} showed a similar trend when measured in the presence of DTT (5 mM), although they differed in the magnitudes. This apparent disparity is likely explained by the fact that the kinetic data for WT + DTT were obtained with a protein sample shortly exposed (< 1 min) to the reducing agent, hence only partially reduced. A fully reduced protein could not be used because *Tc*G6PDH$_L$ then completely loses its activity, in line with prior studies [14] and with our observations on the detrimental effect of lacking structural/regulatory cysteines.

The Cys-triad is located within the Rossmann-fold domain, contiguous in sequence to structural elements that harbor substrate-binding amino acids (Fig. 8). Disruption of the interactions established by these cysteines likely destabilize this important region of the protein, resulting in the kinetic consequences described above. Further crystallographic studies shall reveal the structural role of this Cys-triad residues in Kinetoplastid G6PDHs.

Dynamic active site and N-terminal domain: a catalytic model of *Tc*G6PDH

The kinetic studies highlighted an important role of Kinetoplastid-specific cysteine residues from the N-terminal domain of *Tc*G6PDH, in modulating enzyme activity. In order to provide with mechanistic insights on the residues and structural elements affecting the reaction catalyzed by *Tc*G6PDH, the crystal structures of N-terminally truncated proteins with bound ligands (PDB 6D24 and PDB 5AQ1), were compared to a model of the enzyme-G6P-$NADP^+$ ternary complex ("catalytic model") obtained by molecular dynamics simulations calculated over 80 ns [19]. Relative to the crystallographic structures, both substrates adopted different conformations in the catalytic model, with $NADP^+$ shifted about 3 Å towards the catalytic site and G6P being anchored almost perpendicularly and deeper into the structure core (Fig. 9A). The shift in the position of $NADP^+$ is due to movements of several elements from the Rossmann-fold domain (i.e. helix α2, and loops β1-α2, β2-α3 and β3-α6; Fig. 9A) and do not involve the gain or loss of side chain interactions. In contrast, the conformation observed for G6P in the simulation is facilitated by relaxation of the element connecting strand β6 and helix α9, namely the linker between the N- and the C-terminal domains, and the

consequent rewiring of the substrate´s interaction network (Fig. 9B). In this regard, the π-stacking between Y248 and H309 is lost, which may contribute to destabilize the helical structure of this segment, hence nearby His247 is anticipated to shift 3 Å towards α9, allowing a reorientation of the sugar moiety of G6P, itself anchored to the pocket via H-bonding with K217, H247, Y248 and H309. Because of the partially unfolded conformation of the β6-α9 linker segment, Y248 and K251 are located at unsuitable distances to interact with the phosphate group of G6P (Fig. 9C). Instead, K83 and K84 (located in α2) can interact with the substrate´s phosphate (Fig. 9B), an interaction confirmed by kinetic analysis of mutants [19] but not observed in the substrate-bound crystal structures.

Another region of *Tc*G6PDH that displayed slight differences in the conformation between the crystallographic structure and the molecular dynamics model is loop β5-α8, which contains a proline residue (P218) that in all subunits of apo or holo *Tc*G6PDH is invariably the *cis* isomer (Fig. 9 B and C). This differs with data reported for human and *L. mesenteroides* G6PDH, where this proline has been shown to shuttle from *trans* to *cis* upon formation of the productive ternary complex [26,35,37-40]. The almost exclusive role of the *cis*-Pro in the conformation of the active site was verified by an increase in two orders of magnitude in the apparent k_{cat} and k_{cat}/K_m for both substrates when this residue was exchanged by a valine in *Tc*G6PDH$_L$ (Table 2, P218V mutant). Contiguous to P218 is K217, whose side chain interacts with either G6P O1 and O2 or the carboxylate of D304 (Fig. 9C), according to the crystallographic data. In the catalytic model, the side chain of K217 is almost aligned between the moieties of G6P and $NADP^+$, engaged in the chemical reaction and poised to interact with the sugar. Furthermore, the simulation shows a hydrogen bonding network between the side chains of E216 and Y183 that extends to K217, probably facilitating proton dissociation from the basic residue (Fig. 9B). In fact, mutation of K217 to isoleucine (K217I) impaired catalysis (~10-fold decrease in k_{cat}) and, to a minor degree, the apparent K_m for G6P (3-fold increase) when compared to the wild-type enzyme (Table 2). Further confirming that hydrophobic residues close to the active site favour anchoring of the nicotinamide ring (*e.g.* L80) [19], the P218V and K217I mutants showed increased affinity for $NADP^+$ (1.8-fold). At variance with

H309, which is the catalytic base, K217 and P218 are not directly involved in the chemical steps of the reaction. In this regard, our kinetic and structural analysis suggests that they contribute to substrate-binding and orientation in the transition state.

Overall, and in line with the reaction mechanism obeyed by G6PDH (bi-bi ordered) [20,22,37], our comparative analysis suggests that the acquisition of a catalytically competent conformation in *Tc*G6PDH is likely induced by an ordered binding of substrates. Furthermore, it highlights that the N-terminal region of the Rossmann-fold domain of *Tc*G6PDH may have an important conformational flexibility, amenable to stabilization by forming specific disulphide bonds.

CONCLUSIONS

The biological role of *Tc*G6PDH in redox homeostasis and in trypanosomal drug resistance mechanisms [8,14,16,17] make of this enzyme an attractive target for anti-trypanosomatid drug development. Several 3D structures of *Tc*G6PDH [19,23,29] led us now to a thorough comparison with its human counterpart, pinpointing pathogen-specific features.

The activity of human [41,42], cyanobacteria [43] and plant [44] G6PDH has been shown to benefit from an oligomeric (dimeric > tetrameric) assembly. However, at variance with the *T. cruzi* enzyme, oligomerization of these proteins depends on ligands (substrate, metabolites) and different physicochemical factors. Here we disclosed that *Tc*G6PDH forms highly stable tetramers with a single residue, Arg323, being responsible for stabilizing this oligomeric conformation. Importantly, conversion of *Tc*G6PDH into a predominantly dimeric form, proved detrimental for its enzyme activity. Our data suggest that the dimer-dimer contacts established *via* the R323 salt bridges, are also important to stabilize the R323-containing loop and hence, the portion immediately N-terminal to it (*i.e.* the segment E285-T318), which includes amino acids engaged in G6P-binding and in catalysis. As shown here for the crithidial enzyme, a tetrameric conformation of G6PDH appears to be a common trait of Kinetoplastid G6PDHs, even those that lack R323. In the latter, a downstream and conserved arginine (R331 in *Cf*G6PDH) appears to surrogate the stabilizing role of R323 by forming an inter-subunit salt

bridge with a nearby aspartate (D334) from a neighboring dimer. In contrast, G6PDHs from other Phyla lack basic residues in the equivalent positions altogether. A lineage-specific evolution of Kinetoplastid G6PDHs has apparently favored the acquisition of a stable tetrameric assembly. The activity of the plastidic isoforms of G6PDHs from plants and cyanobacteria are known to be subject of redox control, responding to reducing power requirements during the Calvin cycle for carbon fixation [45]. However, the cysteine residues responsible for such a regulation are not conserved among those organisms [46,47], nor with *Tc*G6PDH, making unlikely the hypothesis of a plastidic origin of the trypanosomal protein, as has been proposed for several other important metabolic enzymes [48]. Within the parasite-exclusive N-terminal extension of *Tc*G6PDH, and out of the several Cys residues exposed to the solvent, we have now found that C8 and C34 are the ones responsible for the formation of an intermolecular disulfide bridge between subunits of the dimer. These two cysteines proved to be key in mediating redox regulation of *Tc*G6PDH activity, as the kinetic parameters of the single or double Cys mutants were impaired with respect to the wild-type enzyme. The precise molecular events underlying the redox-dependent regulation of *Tc*G6PDH$_L$ activity are yet to be discovered. However, our structural and enzyme kinetic data lead us to posit that the reduction of the disulfide bridges from two subunits of the dimer, likely distort the conformation of the mobile N-terminal extension of *Tc*G6PDH$_L$. In turn this would readily translate into conformational rearrangements and/or dynamic modulation of the juxtaposed structural elements, which are directly involved in ligand binding and/or in effecting the accessibility of the substrates to their binding sites. Additional structural stabilization within each protein subunit appears to be provided by a second set of cysteines (C53, C94 and C135) strictly conserved in G6PDHs from Kinetoplastids. The crystal structures of truncated versions of *Tc*G6PDH showed these three cysteines forming intramolecular disulfide bridges (C53-C135 or C94-C135) and the corresponding cysteine point-mutants of the full-length protein proved detrimental for enzyme activity. This suggests a complex inter- and intra-molecular redox regulation/stabilization of the G6PDH activity that shall be further analyzed in future studies.

The stable tetrameric and redox-regulated conformation of G6PDH that evolved in trypanosomes, raises the question about the evolutionary constraints that might have led to divergence with the counterpart from other organisms. Probably, the more challenging growth conditions faced by these unicellular pathogens during their life cycle, acted as a selective pressure for developing a highly stable tetrameric conformation of G6PDH to ensure a steady supply of NADPH and/or ribose-5-phosphate. This evolutionary trait clearly differs from that evolved by G6PDH from several human lineages. Human G6PDH-deficiency, commonly known as favism, is the most frequent enzymopathy associated to unstable enzyme conformations [49]. Several genetic and clinical evidences support that malaria infection acted as a major selective agent for the development of G6PDH-deficiency as this renders erythrocytes unsuited for hosting *Plasmodium* sp. [50-53]. Altogether, this highlights the central role of G6PDH in cell metabolism and its propensity to undergo subtle structural changes with functional consequences. This is in line with the “new view” of protein structure-function evolution [54].

Human and *T. cruzi* G6PDHs share similar backbone structures, but the detailed molecular features presented in this work, as well as in prior studies from our laboratory [19], provide insights into the several regulatory and structural elements to be selectively targeted, as a rational strategy for anti-trypanosome drug development.

EXPERIMENTAL PROCEDURES

Reagents

Molecular biology reagents were purchased from Fermentas (Thermo-Fisher Scientific), New England Biolab, Stratagene and Invitrogen. Chemical reagents were of analytical or higher grade and obtained from Sigma-Aldrich or AppliChem. Antibiotics were purchased from Invitrogen and Sigma-Aldrich. Oligonucleotides were synthesized by IDT. The kits for DNA purification were from Sigma-Aldrich and Invitrogen. All protein purification resins and columns were from General Electric Healthcare Life-Sciences (GE). The brain heart infusion (BHI) broth

and additives from the cell culture medium were purchased from Sigma-Aldrich, and tetracycline-free certified fetal calf serum was from PAA Laboratories.

Plasmids

The constructs for the expression of N-terminally His-tagged full-length (*Tc*G6PDH$_L$; Accession Nr. ABD72517.1) and truncated mutant lacking the first 37 amino acids (Δ37N-*Tc*G6PDH) of *T. cruzi* G6PDH were kindly provided by Dr. J. J. Cazzulo (Universidad Nacional de San Martín-CONICET, Argentina) [14]. The plasmid encoding for N-terminally His-tagged human G6PDH (*Hs*G6PDH, NCBI Nucleotide Reference Sequence NM_000402.3) was provided by Dr. Nial Hamilton (formerly at Manchester University, UK). The sequence encoding for *Crithidia fasciculata* G6PDH (*Cf*G6PDH; Accession Nr. CFAC1_290028300.1, http://tritrypdb.org/tritrypdb/) was de novo synthesized and inserted into pET28a(+) plasmid (Genscript), in frame with a vector sequence that adds an N-terminal 6x His-tag to the recombinant product.

The single Cys^{8}Ser, Cys^{34}Ser, Lys^{217}Iso, Pro^{218}Val, His^{309}Gly, Arg^{323}Gly and Cys^{552}Ser mutants were generated by using the Quick Change site-directed mutagenesis kit (Stratagene, La Jolla, CA, USA) and the construct pET28a(+)-*Tc*G6PDH$_L$ as template with the primer pairs indicated in supplementary Table 1. The PCR were performed in a total reaction volume of 50 µL according to the instructions of the supplier. One Shot® MAX Efficiency® DH5α™-T1R cells were transformed with the mutagenesis reaction. The double mutant C8S/C34S and R323G/C528R were generated using as template the construct pET28a(+)-*Tc*G6PDH$_L$ harbouring the C8S and the R323G mutation, respectively, and the primer pairs Cys^{34}Ser Fwd/Cys^{34}Ser Rev and Cys^{528}Arg Fwd/Cys^{528}Arg Rev (Supplementary Table 1), respectively, and the Quick Change site-directed mutagenesis kit as indicated above.

The correctness of the targeted mutations was confirmed in at least three independent plasmids from each construct by DNA sequencing of the complementary chains (Molecular Biology Unit, Institut Pasteur de Montevideo, Uruguay or Macrogen, Korea).

Expression and purification of recombinant proteins

E. coli Tuner (DE3) cells were transformed with the expression plasmids encoding for wild-type G6PDH from different organisms or the corresponding mutant versions. An overnight culture of transformed bacteria in LB medium with 50 µg/L kanamycin was inoculated at a ratio 1:100 in ZYM-5052 auto-induction medium added of 50 µg/L kanamycin and cell grow extended for 48 h at 25°C and 200 rpm. Cells were harvested by centrifugation (5000 *g*, 10 min, 4°C), and suspended in 50 mM Tris, pH 8.0, 500 mM NaCl, 5 mM $MgCl_2$ (buffer A) plus 1 mM PMSF, 40 µg/ml TLCK, 150 nM pepstatin, 4 nM cystatin, or Complete™ Protease Inhibitor Cocktail (Sigma-Aldrich). Hen egg-white lysozyme was added (final concentration 1 mg/ml) and incubated for 60 min at 8 C°. After disruption by three cycles of sonication (30 pulses per minute at 45-70% amplitude) using a macrotip in a Digital Sonifier 450 (Branson), the cell lysate was centrifuged at 15000 *g* (15 min, 4°C) and the supernatant was further cleared of debris by centrifugation at 20000 *g* (30 min, 4°C) and filtration through a 0.45 µm filter (Millipore). The cleared lysate was loaded onto a HisTrap column (GE) pre-equilibrated with buffer A. The column was washed with 10 and 5 column volume of buffer A and 5 mM imidazole in buffer A, respectively, and the protein eluted with 500 mM imidazole in buffer A. The fractions containing the recombinant protein were collected, concentrated via ultrafiltration (10-kDa filter cutoff), and run on a Superdex 200 10/300 GL column (GE) pre-equilibrated with buffer A. Fractions containing the protein of interest, as assessed by Coomassie blue-stained SDS-PAGE (10% polyacrylamide), were collected, tested for enzyme specific activity (see below), concentrated to 0.5 mg/mL and stored at 4°C. Protein concentration was determined by the bicinchoninic acid assay or absorbance at 280 nm considering the molar extinction coefficient as calculated from the protein sequence.

Analytical size exclusion chromatography

The oligomeric state of the different recombinant proteins characterized in this work was studied by analytical gel-filtration chromatography on a Superdex 200 10/300 GL column (GE) coupled to an AKTA FPLC system (both from GE-Health Care) with online UV–visible detection. All chromatography experiments were performed at room temperature (RT) in 50

mM Tris.HCl pH 7.5, 0.5 M NaCl, 5 mM $MgCl_2$ (reaction buffer), at a constant flow of 0.5 mL/min. The column was calibrated under identical running conditions with molecular weight standards (ovalbumin, conalbumin, aldolase, ferritin and tyroglobulin, ranging 43–669 kDa). To test the effect of different ligands on protein oligomerization, *Tc*G6PDH$_L$ (50-150 µg/mL) was incubated for 30 min at 4°C in reaction buffer added of 5 mM NADP, 5 mM G6P or 100 µM DHEA, and then resolved by gel filtration in reaction buffer containing the corresponding additives at identical concentrations. Similar amounts of protein were also subjected to gel filtration under different physicochemical conditions that involved the presence of a reducing agent (5 mM DTT), high ionic strength (1 M NaCl), and non-ionic (0.1 % (v/v) Triton X-100) and/or ionic (0.1 % (w/v) SDS) detergent. The effect of pH on *T. cruzi* and *C. fasciculata* G6PDHs' oligomeric structures, was studied using 50 mM MES at pH 5.5 or 6.5 with 0.5 M NaCl and 5 mM $MgCl_2$. Protein elution was monitored online by 280 nm absorbance. The peaks of interest were subjected to enzymatic tests (see below) and denaturing 10% polyacrylamide gel electrophoresis under reducing (5% (v/v) ß-mercaptoethanol) and non-reducing conditions.

Structure determination

The crystallization conditions and X-ray diffraction data collection for recombinant Δ37N-*Tc*G6PDH in its apo-form and bound to glucose-6-phosphate were previously described in [23]. Initial phases for the apo-form model were obtained by molecular replacement with PHASER [55], using the main chain atoms of 1QKI chain A (human G6PDH NADP+ complex) [30] as search probe. The resulting model was used in initial rigid body refinement against data from *T. cruzi* G6P-G6PDH co-crystal using REFMAC5 [56]. Cycles of reciprocal space refinement were performed with REFMAC5 and later with Buster [57] using local non-crystallographic symmetry restraints and alternate TLS refinement. Sigma-weighted (2mFo-DFc and mFo-DFc) electron density maps were used in Coot [58] to guide manual protein rebuilding and addition of solvent and ligand molecules. Validation was performed with Coot during model rebuilding and finally with MolProbity [59].

*Cf*G6PDH structure was generated by structure homology-modelling using the SWISS-MODEL server [60] and PDB 6D24 as template.

Protein and kinetics assays

Protein concentration was determined by the BCA method (Bicinchoninic Acid Protein Assay Kit, Sigma) using bovine serum albumin (BSA) as standard. G6PDH activity was determined at ~ 25°C by monitoring NADPH (ε_{340} (NADPH) = 6,220 M^{-1} cm^{-1}) formation at 340 nm. All reactions were performed in 50 mM Tris.HCl pH 7.5, 5 mM $MgCl_2$, in 150 µL final volume, and started by addition of G6P. For standard assays, $NADP^+$ and G6P were used at fixed concentrations of 500 µM and 6 mM, respectively, and with variable protein concentrations (10-897 nM). For determination of the apparent Michaelis constants (K_m^{app}) and maximum apparent velocities (V_{max}^{app}), each substrate was tested at five different concentrations (15 to 6000 µM for G6P, and 1 to 800 µM for $NADP^+$) under fixed and saturating concentration of the second substrate involved (1 to 15 mM for G6P, and 500 µM for $NADP^+$), using protein concentrations of 15 nM (for *Tc*G6PDH$_L$), 16 nM (Δ37N-*Tc*G6PDH), 120 nM (C8S-*Tc*G6PDH$_L$), 160 nM (H309G-*Tc*G6PDH$_L$), 150 nM (K217I-*Tc*G6PDH$_L$), 138 nM (P218V-*Tc*G6PDH$_L$), 613 nM (R323R-*Tc*G6PDH$_L$), 897 nM (R323R/C528R-*Tc*G6PDH$_L$), 780 nM (C53S-*Tc*G6PDH$_L$), 549 nM (C94S-*Tc*G6PDH$_L$), 212 nM (C135S-*Tc*G6PDH$_L$) and 339 nM (C528R-*Tc*G6PDH$_L$). For determination of kinetic parameters under reducing conditions, the enzymatic assays were performed in the presence of 5 mM DTT. All measurements were performed at least in triplicate using a Cary 50 Bio spectrophotometer (Agilent Technologies, Santa Clara, CA, USA at RT. The initial rates were determined with the Origin Pro 8.0 software (OriginLab Corporation, Northampton, MA, USA), and the apparent kinetic constants were calculated by nonlinear regression with the equation below using the GraphPad Prism 5.0 software (GraphPad Inc., San Diego, CA, USA).

$$v = V_{max}^{app} \frac{[S]}{K_M^{app} + [S]}$$

where V_{max}^{app} is the apparent maximum reaction rate, [*S*] is the concentration of either NADP+ or G6P) and K_m^{app} is the apparent Michaelis constant. This approach, which is widely used for the analysis of the kinetics of G6P dehydrogenases (Igolillo-Esteve, 2006), is herein complemented with the analysis of the data given the ordered bisubstrate biproduct general model [61].

Western blots

Anti-*Tc*G6PDH$_L$ serum was produced in mice (strain Balbc/J) using a standard immunization protocol with purified recombinant *Tc*G6PDH$_L$ as antigen, approved by the Institut Pasteur de Montevideo Committee on Animal Use and Ethics (CEUA Protocol # 005-14). Mice were obtained from the in-house *specific pathogen free* animal facility (Transgenic and Experimental Animal Unit, Institut Pasteur de Montevideo). The *Tc*G6PDH$_L$ cysteine mutants C8S, C34S and C8S/C34S, were expressed and purified as described above, and stored for one week at 4°C in reaction buffer lacking any reducing agent. The different mutants at 2.5 µM were incubated 30 min in buffer A with 150 µM DTT, the reducing agent was then removed using a NAP-5 desalting column (GE-Healthcare) pre-equilibrated in buffer A. A fraction of the DTT-reduced samples was stored on ice for SDS-PAGE analysis, and the remaining fraction was oxidized at 4 °C with 150 µM GSSG during 90 min. Each protein (300 ng) issued from non-reduced, DTT reduced and GSSG-oxidized samples, was separated by SDS-PAGE (10% polyacrylamide) under non-reducing conditions and transferred to a polyvinylidene fluoride (PVDF) membrane (GE-Healthcare). The membrane was blocked overnight at 4°C in PBS + 0.2 % (v/v) Tween-20 (PBS-T) and 5 % (w/v) non-fat dry milk, washed with PBS-T and incubated with polyclonal mouse anti-*Tc*G6PDH$_L$ serum diluted 1:1000 in PBS-T at room temperature for 2 h. After three washing steps with PBS-T for 5 min each, the membrane was incubated for 1 h at RT with horseradish peroxidase-conjugated

goat anti-mouse IgG (Amersham Biosciences, Buckinghamshire, England) diluted 1:10,000 in PBS-T. The membrane was extensively washed in PBS-T prior to chemoluminiscent detection of reactive bands with the Amersham ECL™ Western Blotting Detection Reagents (GE Healthcare) according to the manufacturer's instructions. Films (Amersham hyperfilm ECL, GE Healthcare) were exposed to the membranes during different times (1, 5 and 10 minutes) and developed for 1 min in developing solution (Sigma).

ACCESION NUMBERS

Structural coordinates of free *Trypanosoma cruzi* G6PDH, and in complex with glucose 6-phosphate, have been deposited in the Protein Data Bank with IDs: 6D23 and 6D24, respectively.

ACKNOWLEDGEMENTS

This work was supported by a grant from the Agencia Nacional de Investigación e Innovación (ANII; Innova Uruguay, Agreement No. DCI-ALA/2007/19.040 between Uruguay and the European Commission) to MAC. CO and MAC acknowledge the financial support from ANII (POS_NAC_2012_1_8803 and Comisión Académica de Posgrados, Universidad de la República, Uruguay) and PEDECIBA. Andrea Medeiros (Lab. Redox Biology of Trypanosomes) and Gabriel Fernández (Transgenic and Animal Experimentation Unit, Institut Pasteur de Montevideo) are gratefully acknowledged for technical assistance during production of *Tc*G6PDH antiserum, and Nicole Larrieux (Protein Crystallography Facility, Institut Pasteur de Montevideo) for assistance with crystallization and X-ray diffraction data collection.

Conflict of interest

The authors declare that they have no conflicts of interest with the contents of this article.

Author contributions

CO conducted most experiments, analyzed the results, contributed to paper writing. HB contributed to structure refinement and analyzed data. AB contributed to structure refinement, analyzed data and wrote the paper. MAC conceived the idea for the project, performed the experimental designs, analyzed data and wrote the paper. All authors discussed the data and read the manuscript.

REFERENCES

[1] Krauth-Siegel RL, Comini MA (2008) Redox control in trypanosomatids, parasitic protozoa with trypanothione-based thiol metabolism. Biochim Biophys Acta. 1780(11):1236-1248.

[2] Irigoín F, Cibils L, Comini MA, Wilkinson SR, Flohé L, Radi R (2008) Insights into the redox biology of Trypanosoma cruzi: Trypanothione metabolism and oxidant detoxification. Free Radic Biol Med. 45(6):733-742.

[3] Barderi P, Campetella O, Frasch AC, Santomé JA, Hellman U, Pettersson U, Cazzulo JJ (1998) The NADP+-linked glutamate dehydrogenase from Trypanosoma cruzi: sequence, genomic organization and expression. Biochem J. 330(2): 951-958.

[4] Maugeri DA, Cazzulo JJ. (2004) The pentose phosphate pathway in Trypanosoma cruzi FEMS Microbiol Lett. 1;234(1):117-23

[5] Esteve MI, Cazzulo JJ (2004) The 6-phosphogluconate dehydrogenase from Trypanosoma cruzi: the absence of two inter-subunit salt bridges as a reason for enzyme instability. Mol Biochem Parasitol.133(2):197-207.

[6] Leroux AE, Maugeri DA, Cazzulo JJ, Nowicki C (2011) Functional characterization of NADP-dependent isocitrate dehydrogenase isozymes from Trypanosoma cruzi. Mol Biochem Parasitol. 177(1):61-4.

[7] Leroux AE, Maugeri DA, Opperdoes FR, Cazzulo JJ, Nowicki C (2011) Comparative studies on the biochemical properties of the malic enzymes from Trypanosoma cruzi and Trypanosoma brucei. FEMS Microbiol Lett. 314(1):25-33.

[8] Gupta S, Cordeiro AT, Michels PA (2011) Glucose-6-phosphate dehydrogenase is the target for the trypanocidal action of human steroids. Mol Biochem Parasitol. 176(2):112-5.

[9] Spaans SK, Weusthuis RA, van der Oost J, Kengen SW (2015) NADPH-generating systems in bacteria and archaea. Front. Microbiol. 6:742.

[10] Comini MA, Ortíz C, Cazzulo JJ. Drug Targets in Trypanosomal and Leishmanial Pentose Phosphate Pathway. In: Jäger T, Koch O, Flohé L, editors. Trypanosomatid Diseases [Internet]. Wiley-VCH Verlag GmbH & Co. KGaA; 2013. p. 297–313.

[11] Kovářová J, Barrett MP (2016) The Pentose Phosphate Pathway in Parasitic Trypanosomatids. Trends Parasitol. 32(8):622-634

[12] Mancilla R, Naquira C (1964) Comparative metabolism of C14-glucose in two strains of Trypanosoma cruzi. J Protozool. 11:509-513.

[13] Finzi JK, Chiavegatto CW, Corat KF, Lopez JA, Cabrera OG, Mielniczki-Pereira AA, Colli W, Alves MJ, Gadelha FR (2004) Trypanosoma cruzi response to the oxidative stress generated by hydrogen peroxide. Mol Biochem Parasitol. 133(1):37-43

[14] Igoillo-Esteve M, Cazzulo JJ (2006) The glucose-6-phosphate dehydrogenase from Trpanosoma cruzi: its role in the defense of the parasite against oxidative stress. Mol Biochem Parasitol. 149(2):170-81.

[15] Mielniczki-Pereira AA, Chiavegatto CM, López JA, Colli W, Alves MJ, Gadelha FR (2007) Trypanosoma cruzi strains, Tulahuen 2 and Y, besides the difference in resistance to oxidative stress, display differential glucose-6-phosphate and 6-phosphogluconate dehydrogenases activities. Acta Trop. 101(1):54-60.

[16] Ghosh AK, Sardar AH, Mandal A, Saini S, Abhishek K, Kumar A, Purkait B, Singh R, Das S, Mukhopadhyay R, Roy S, Das P (2015) Metabolic reconfiguration of the central glucose metabolism: a crucial strategy of Leishmania donovani for its survival during oxidative stress. FASEB J. 29(5):2081-98.

[17] Ghosh AK, Saini S, Das S, Mandal A, Sardar AH, Ansari MY, Abhishek K, Kumar A, Singh R, Verma S, Equbal A, Ali V, Das P (2017) Glucose-6-phosphate dehydrogenase and Trypanothione reductase interaction protects Leishmania donovani from metalloid mediated oxidative stress. Free Radic Biol Med. 106:10-23.

[18] Mercaldi GF, Ranzani AT, Cordeiro AT (2014) Discovery of new uncompetitive inhibitors of glucose-6-phosphate dehydrogenase. J Biomol Screen. 19(10):1362-71.

[19] Ortiz C, Moraca F, Medeiros A, Botta M, Hamilton N, Comini MA (2016) Binding Mode and Selectivity of Steroids towards Glucose-6-phosphate Dehydrogenase from the Pathogen Trypanosoma cruzi. Molecules. 21(3):368.

[20] Funayama S, Funayama S, Ito IY, Veiga LA (1977) Trypanosoma cruzi: kinetic properties of glucose-6-phosphate dehydrogenase. Exp Parasitol. 43(2):376-81

[21] Heise, N. and Opperdoes, F.R. (1999) Purification, localization and characterization of glucose-6-phosphate dehydrogenase of Trypanosoma brucei. Mol. Biochem. Parasitol., 99, 21–32.

[22] Cordeiro AT, Thiemann OH, Michels PA (2009) Inhibition of Trypanosoma brucei glucose-6-phosphate dehydrogenase by human steroids and their effects on the viability of cultured parasites. Bioorg Med Chem. 17(6):2483-2489.

[23] Ortíz, C., Larrieux, N., Medeiros, A., Botti,H., Comini, M., and Buschiazzo, A. (2011) Expression, crystallization and preliminaryX-ray crystallographic analysis of glucose-6-phosphate dehydrogenase from the humanpathogen Trypanosoma cruzi in complex with substrate. Acta. Crystallogr. F, 67, 1457–1461.

[24] Shreve, D.S., and Levy, H.R. (1977). On the molecular weight of human glucose 6-phosphate dehydrogenase. Biochem. Biophys. Res. Commun. *78*, 1369–1375.

[25] Schaeffer, F & Stanier, RY. (1978) Glucose-6- phosphate dehydrogenase of anabaena sp. kinetics and molecular properties. Archives of microbiology 116, 9-19.

[26] Rowland P, Basak AK, Gover S, Levy HR, Adams MJ (1994) The three-dimensional structure of glucose 6-phosphate dehydrogenase from Leuconostoc mesenteroides refined at 2.0 A resolution. Structure 2(11):1073-87

[27] Sundaram S, Karakaya H, Scanlan DJ, Mann NH (1998) Multiple oligomeric forms of glucose-6-phosphate dehydrogenase in cyanobacteria and the role of OpcA in the assembly process. Microbiology 144 (Pt 6):1549-56.

[28] Comakli, V, Akkemik, E, Ciftci, M, and Kufrevioglu, OI. (2015). Purification and characterization of glucose 6-phosphate dehydrogenase enzyme from rainbow trout (Oncorhynchus mykiss) liver and investigation of the effects of some metal ions on enzyme activity. Toxicol. Ind. Health *31*, 403–411.

[29] Mercaldi GF, Dawson A, Hunter WN, Cordeiro AT (2016) The structure of a Trypanosoma cruzi glucose-6-phosphate dehydrogenase reveals differences from the mammalian enzyme. FEBS Lett. 590(16):2776-86.

[30] Au SW, Gover S, Lam VM, Adams MJ (2000) Human glucose-6-phosphate dehydrogenase: the crystal structure reveals a structural NADP(+) molecule and provides insights into enzyme deficiency. Structure 8(3):293-303.

[31] Cohen P, Rosemeyer MA (1975) Glucose-6-phosphate dehydrogenase from human erythrocytes. Methods Enzymol 41:208-14.

[32] Bonsignore A, Cancedda R, Lorenzoni I, Cosulich ME, De Flora A (1971) Human erythrocyte glucose 6-phosphate dehydrogenase. Physical properties. Biochem Biophys Res Commun. 43(1):94-101.

[33] Wang XT, Engel PC (2009) Clinical mutants of human glucose 6-phosphate dehydrogenase: impairment of NADP(+) binding affects both folding and stability. Biochim Biophys Acta. 1792(8):804-9.

[34] Wang XT, Chan TF, Lam VM, Engel PC (2008) What is the role of the second "structural" NADP+-binding site in human glucose 6-phosphate dehydrogenase? Protein Sci. 17(8):1403-11.

[35] Kotaka M, Gover S, Vandeputte-Rutten L, Au SW, Lam VM, Adams MJ (2005) Structural studies of glucose-6-phosphate and NADP+ binding to human glucose-6-phosphate dehydrogenase. Acta Crystallogr D Biol Crystallogr. 61(Pt 5):495-504.

[36] Filosa S, Calabrò V, Vallone D, Poggi V, Mason P, Pagnini D, Alfinito F, Rotoli B, Martini G, Luzzatto L, Battistuzzi G (1992) Molecular basis of chronic non-spherocytic haemolytic anaemia: a new G6PD variant (393 Arg----His) with abnormal KmG6P and marked in vivo instability. Br J Haematol 80(1):111-6.

[37] Cosgrove MS, Naylor C, Paludan S, Adams MJ, Levy HR (1998) On the mechanism of the reaction catalyzed by glucose 6-phosphate dehydrogenase. Biochemistry 37(9):2759-67.

[38] Cosgrove MS, Gover S, Naylor CE, Vandeputte-Rutten L, Adams MJ, Levy HR (2000) An examination of the role of asp-177 in the His-Asp catalytic dyad of Leuconostoc mesenteroides glucose 6-phosphate dehydrogenase: X-ray structure and pH dependence of kinetic parameters of the D177N mutant enzyme. Biochemistry 39(49):15002-11

[39] Naylor CE, Gover S, Basak AK, Cosgrove MS, Levy HR, Adams MJ (2001) NADP+ and NAD+ binding to the dual coenzyme specific enzyme Leuconostoc mesenteroides glucose 6-phosphate dehydrogenase: different interdomain hinge angles are seen in different binary and ternary complexes. Acta Crystallogr D Biol Crystallogr. 57(Pt 5):635-48.

[40] Naylor CE, Gover S, Basak AK, Cosgrove MS, Levy HR, Adams MJ (2001) NADP+ and NAD+ binding to the dual coenzyme specific enzyme Leuconostoc mesenteroides glucose 6-phosphate dehydrogenase: different interdomain hinge angles are seen in different binary and ternary complexes. Acta Cryst. D57: 635-648.

[41] Cohen P, Rosemeyer MA (1968) The molecular weight and subunit structure of glucose-6-phosphate dehydrogenase from human erythrocytes. FEBS Lett. 1(3):147-149.

[42] Ranzani AT, Cordeiro AT (2017) Mutations in the tetramer interface of human glucose-6-phosphate dehydrogenase reveals kinetic differences between oligomeric states. FEBS Lett. 591(9):1278-1284.

[43] Hagen KD, Meeks JC (2001) The unique cyanobacterial protein OpcA is an allosteric effector of glucose-6-phosphate dehydrogenase in Nostoc punctiforme ATCC 29133. J Biol Chem. 276(15):11477-86.

[44] Hong ZQ, Copeland L (1991) Isoenzymes of glucose 6-phosphate dehydrogenase from the plant fraction of soybean nodules. Plant Physiol 96(3):862-7.

[45] Oesterhelt C, Klocke S, Holtgrefe S, Linke V, Weber AP, Scheibe R (2007) Redox regulation of chloroplast enzymes in Galdieria sulphuraria in view of eukaryotic evolution. Plant Cell Physiol. 48(9):1359-73.

[46] Udvardy J, Borbely G, Juhász A, Farkas GL (1984) Thioredoxins and the redox modulation of glucose-6-phosphate dehydrogenase in Anabaena sp. strain PCC 7120 vegetative cells and heterocysts. J Bacteriol 157(2):681-3.

[47] Wenderoth I, Scheibe R, von Schaewen A (1997) Identification of the cysteine residues involved in redox modification of plant plastidic glucose-6-phosphate dehydrogenase. J Biol Chem 272(43):26985-90.

[48] Hannaert V, Saavedra E, Duffieux F, Szikora JP, Rigden DJ, Michels PA, Opperdoes FR (2003) Plant-like traits associated with metabolism of Trypanosoma parasites. Proc Natl Acad Sci U S A. 100(3):1067-71.

[49] Beutler E (1994) G6PD deficiency. Blood 84: 3613–3636.

[50] Allison AC, Clyde DF (1961) Malaria in African children with deficient erythrocyte glucose-6 phosphate dehydrogenase. Br. Med. J. 1: 1346–1349.

[51] Roth EF, Raventos-Suarez C, Rinaldi A, Nagel RL (1983) Glucose-6-phosphate dehydrogenase deficiency inhibits in vitro growth of Plasmodium falciparum. Proc. Natl. Acad. Sci. U. S. A. 80: 298–299.

[52] Ruwende C, Khoo SC, Snow RW, Yates SN, Kwiatkowski D, Gupta S, Warn P, Allsopp CE, Gilbert SC, Peschu N (1995) Natural selection of hemi- and heterozygotes for G6PD deficiency in Africa by resistance to severe malaria. Nature 376: 246–249.

[53] Tishkoff SA, Varkonyi R, Cahinhinan N, Abbes S, Argyropoulos G, Destro-Bisol G, Drousiotou A, Dangerfield B, Lefranc G, Loiselet J, Piro A, Stoneking M, Tagarelli A, Tagarelli G, Touma EH, Williams SM, Clark AG (2001). Haplotype diversity and linkage disequilibrium at human G6PD: recent origin of alleles that confer malarial resistance. Science 293: 455–462.

[54] James LC, Tawfik DS (2003). Conformational diversity and protein evolution — a 60-year-old hypothesis revisited. Trends Biochem. Sci. 28(7):361-368.

[55] McCoy AJ, Grosse-Kunstleve RW, Adams PD, Winn MD, Storoni LC, Read RJ (2007) Phaser crystallographic software. J Appl Crystallogr. 40(Pt 4):658-674.

[56] Murshudov GN, Skubák P, Lebedev AA, Pannu NS, Steiner RA, Nicholls RA, Winn MD, Long F, Vagin AA (2011) REFMAC5 for the refinement of macromolecular crystal structures. Acta Crystallogr D Biol Crystallogr. 67(Pt 4):355-67.

[57] Smart OS, Womack TO, Flensburg C, Keller P, Paciorek W, Sharff A, Vonrhein C, Bricogne G (2012) Exploiting structure similarity in refinement: automated NCS and target-structure restraints in BUSTER. Acta Crystallogr D Biol Crystallogr. 68(Pt 4):368-80.

[58] Emsley P, Lohkamp B, Scott WG, Cowtan K (2010) Features and development of Coot. Acta Crystallogr D Biol Crystallogr. 66(Pt 4):486-501.

[59] Chen VB, Arendall WB 3rd, Headd JJ, Keedy DA, Immormino RM, Kapral GJ, Murray LW, Richardson JS, Richardson DC (2010) MolProbity: all-atom structure validation for macromolecular crystallography. Acta Crystallogr D Biol Crystallogr. 66(Pt 1):12-21.

[60] Waterhouse A, Bertoni M, Bienert S, Studer G, Tauriello G, Gumienny R, Heer FT, de Beer TAP, Rempfer C, Bordoli L, Lepore R, Schwede T (2018) SWISS-MODEL: homology modelling of protein structures and complexes. Nucleic Acids Res. 46(W1), W296-W303.

[61] Cleland WW (1967) Steady state kinetics. Adv. Enzymol. 29:1–65.

Table 1. X-ray diffraction data processing and model refinement statistics.

	TcG6PDHΔN37 - free enzyme (apo)	TcG6PDHΔN37 - in complex with Glc-6-P (G6P)
Data collection and processing		
Wavelength (Å)	1.000	1.000
Space group	$P2_1$	$P2_1$
Cell parameters		
***a b c* (Å)**	96.6 133.0 107.8	96.8 133.0 107.7
α β γ (°)	90.0 100.1 90.0	90.0 100.3 90.0
Resolution range (Å)	29.629 – 2.850 (3.00-2.85)*	67.36 – 3.35 (3.53-3.35)*
Unique reflections	62028 (9028)	38508 (5606)
Completeness (%)	99.1 (99.2)	99.5 (99.9)
Multiplicity	3.5 (3.7)	3.5 (3.6)
Rmerge †	0.14 (0.50)	0.21 (0.45)
Rpim §	0.09 (0.32)	0.13 (0.28)
Mean I/σ(I)	7.1 (2.3)	5.5 (2.9)
$CC_{1/2}$	0.984 (0.797)	0.959 (0.837)
Refinement		
Resolution range (Å)	29.63 – 2.85	34.16 – 3.35
Number of reflections used (working set / free set)	60752 / 1257	37660 / 796
R_{cryst} / R_{free} ¶	0.204 / 0.249	0.205 / 0.254
Wilson B / Average B ($Å^2$)	61.2 / 44.3	50.7 / 36.6
Number of refined atoms (protein/ligand/water)	15441 / 263 / 75	15634 / 270 / 47
RMSD bond length (Å)	0.01	0.01
RMSD bond angle (°)	1.2	1.2
Estimated coordinate error DPI based on R_{free} (Å)	0.3	0.5
Ramachandran plot (% residues in favored regions / outliers)	94.43 / 0.36	92.21 / 0.91

* Values in parentheses are for highest-resolution shell.

† $R_{merge} = \Sigma_{hkl} \Sigma_i |I_i - \langle I \rangle| / \Sigma_{hkl} \Sigma_i I_i$,
I_i is the intensity of the i^{th} observation of reflection hkl, $\langle I \rangle$ is the mean intensity of all observations of reflection hkl, summation Σ_{hkl} extends over all reflections (hkl), summation Σ_i is taken over all observations of each reflection (i), respectively.

§ $R_{pim} = \Sigma_{hkl} [n/(n-1)]^{1/2} \Sigma_i | I_i - \langle I \rangle | / \Sigma_{hkl} \Sigma_i I_i$
n is the multiplicity for each reflection hkl, other variables as defined for R_{merge}.

¶ $R = \Sigma_{hkl} |F_o - F_c| / \Sigma_{hkl} F_o$,
R_{cryst} and R_{free} were calculated using the working and test hkl reflection sets, respectively.

Table 2. Apparent kinetic parameters for different versions of recombinant *Tc*G6PDH.

	G6P			NAP		
TcG6PDH[a]	K_m (μM)	k_{cat} (s^{-1})	k_{cat}/K_m ($\mu M^{-1}.s^{-1}$)	K_m (μM)	k_{cat} (s^{-1})	k_{cat}/K_m ($\mu M^{-1}.s^{-1}$)
WT	77±20	62±3	0.81	16±3	52±2	3.3
R323G	504±66	4.8±0.1	0.0095	69±9	5.7±0.2	0.08
R323G/C528R	105±22	1.10±0.04	0.01	21±4	1.70±0.05	0.07
C528R	70±13	63±2	0.87	25±5	72±2	2.9
WT + DTT	318±49	108±4	0.34	39±6	82±3	2.1
Δ37N	275±115	154±16	0.56	18±5	121±6	6.7
C8S	332±32	56±1	0.17	80±6	59±1	0.73
C8S/C34S	98±11	81±2	0.82	84±7	92±2	1.1
C34S	130±9	88±2	0.68	50±6	92±2	1.8
C53S	1545±277	2.9±0.2	0.0019	>334±86	2.1±0.2	0.0063
C94S	178±92	1.1±0.1	0.0062	>622±360	2.1±0.6	0.0034
C135S	679±105	64±3	0.094	>610±114	95±8	0.156
H309G	185±33	0.19±0.01	0.001	18±5	0.15±0.01	0.01
P218V	123±16	0.35±0.01	0.003	9±1	0.23±0.01	0.03
K217I	226±34	6.5±0.3	0.029	9±1	4.4±0.1	0.49

[a] The different forms of TcG6PDH evaluated correspond to: WT, *Tc*G6PDH$_L$; WT + DTT, *Tc*G6PDH$_L$ assayed in the presence of DTT (5 mM); Δ37N, N-terminal truncated mutant of *Tc*G6PDH; C8S, C34S, C8S/C34S, R323G, R323G/C528R, P218V, H309G and K217I are point mutants of *Tc*G6PDH$_L$. The values are expressed as the mean ± the standard deviation (n ≥ 3).

Figure Legends

Figure 1. Tridimensional structure and oligomeric organization of G6P-bound Δ37N-G6PDH from *T. cruzi*. A) Cartoon representation of Δ37N-*Tc*G6PDH tetramer with, **B)** top view displaying the 40° angle difference between dimers´ axis (dimer 1, chain A and chain D, is shown as cartoon and dimer 2, chain B and chain C, is shown as surface), and **C)** monomer with bound G6P. For all figures, the N-terminal Rossmann-fold domain is colored in dark grey, whereas the C-terminal domain is shown with different colors according to the subunit (blue: chain A, green: chain B, yellow: chain C, and red: chain D). G6P atoms are depicted as spheres without hydrogens (green: carbon, red: oxygen and orange: phosphate). The elements conforming the secondary structure of *Tc*G6PDH are numbered accordingly.

Figure 2. Multiple sequence alignment of selected glucose-6-phosphate dehydrogenases from different Phyla. The amino acid sequences for G6PDH shown correspond to *Trypanosoma cruzi* (Tc, Acc. # Q1WBU6), *Trypanosoma brucei* (Tb, Acc. # Q9GRG7), *Leishmania infantum* (Li, Acc. # A2CIJ8), *Homo sapiens* (Hs, Acc. # P11413), *Leuconostoc mesenteroides* (Lm, Acc. # P11411), *Salmonella typhimurium* (St, Acc. # Q8ZNW2), chloroplastic *Solanum tuberosum* (cSt, Acc. # Q43839), chloroplastic *Arabidopsis thaliana* (cAt, Acc. # Q43727), and *Plasmodium falciparum* (Pf, Acc. # Q8IKU0). Residues strictly conserved in all sequences are highlighted with a black background while those conserved in at least 7 out of 9 sequences are shown in bold letters. The secondary structure elements of Δ37N-*Tc*G6PDH with bound G6P (PDB 6D24) are displayed above the sequence alignment. The black and grey lines indicate the N-terminal V52-K84 and E285-R323 regions that may play an allosteric role in *Tc*G6PDH activity. At the bottom of the alignment, the black circle, the empty circle, the asterisk and the arrow indicate residues involved in ionic interactions to stabilize the dimer-dimer contacts, mutated in this study, interacting with G6P and the position of R323, respectively. Residues participating in dimer-dimer salt bridges in *Tc*G6PDH are framed in red (R323-D332 and R323-E333) and light blue (R265-D390 and K321-D390) and for *Hs*G6PDH are framed in yellow (K275-E347) and green (K290-E287).

Figure 3. Size exclusion chromatography analysis of recombinant *Tc*G6PDH$_L$. The full-length form of *Tc*G6PDH (0.8-2.4 μM) was gel filtrated on a Superdex G200 resin (10/300 column) pre-equilibrated in reaction buffer (Tris 50 mM, pH 7.5, NaCl 0.5 M and $MgCl_2$ 5 mM) containing saturating concentrations of different ligands: **A)** DHEA 100 μM (dotted line; retention volume, rv, of 11.2 mL ≅ 240 kDa), NADP 5 mM (dot and dash line, rv =11.3 mL ≅ 230 kDa), or G6P 5 mM (black line, rv = 10.8 mL ≅ 286 kDa), or under different physicochemical conditions: **B)** reaction buffer lacking magnesium (dotted line, rv = 10.8 mL ≅ 286 kDa), DTT 5 mM (black line, rv = 11.2 mL ≅ 240 kDa) and NaCl 1 M (black dot and dash line, rv = 11.2 mL ≅ 240 kDa). For both plots, the head arrow indicate the position at which the peak of the non-treated *Tc*G6PDH$_L$ elutes in reaction buffer (control, rv = 11.2 mL ≅ 240 kDa). A representative chromatogram (n ≥ 2) for each condition is shown. For **A)**, the right Y-axis scale corresponds to the sample run in the presence of G6P, while the left Y-axis scale corresponds to the samples run in the presence of DHEA and NADP.

Figure 4. Tetramer interface of *Tc*G6PDH. A) Critical residues involve in formation of salt bridges between dimers of *Tc*G6PDH (PDB 6D24) are shown in green (chain A with transparent surface and backbone shown as cartoon with N- and C-terminal domains colored in black and red, respectively) and blue (chain D shown as surface with N and C-terminal domain colored in grey and pale green, respectively) sticks. Residues non-conserved in *Hs*G6PDH are labeled in red (R323 and D390). The inset shows the salt bridges formed between R323 and D332 and E333 from subunit A and B (green and red cartoon backbone). **B)** *Tc*G6PDH$_L$ was gel filtrated on a Superdex G200 (10/300 column) equilibrated at pH 7.5 (dotted line; rv 11.2 mL ≅ 240 kDa) and pH 5.5 (black line; rv = 11.8 mL ≅ 168 kDa). The Arg323Gly *Tc*G6PDH$_L$ mutant was separated in the same column equilibrated in reaction buffer without (dash and dot line; rv = 12.5 mL ≅ 135 kDa) and with DTT 5 mM (dark grey line; rv = 12.7 mL ≅ 124 kDa). The arrows indicate the position of the peaks corresponding to the molecular weight standards used for column calibration (thyroglobulin Mr 669 kDa, aldolase Mr 158 kDa and albumin 75 kDa). α_4 and α_2 denote the theoretical positions at which the

tetrameric and dimeric species, respectively, of TcG6PDH$_L$ are expected to elute. A representative chromatogram (n ≥ 2) for each condition is shown. The left Y-axis scale corresponds to the sample run at pH 7.5 (dotted line), whereas the right Y-axis scale refers to the other samples.

Figure 5. G6PDH from *C. fasciculata* forms less stable tetramers than the trypanosomal homologue. A) Size exclusion chromatography analysis of recombinant *Cf*G6PDH$_L$. *Cf*G6PDH$_L$ (24 uM) was reduced (5 mM DTT, 15 min) and gel filtrated on a Superdex G200 resin (10/300 column) pre-equilibrated in reaction buffer (Tris 50 mM, pH 8, NaCl 0.5 M and MgCl2 5 mM) containing DTT 5 mM (black dot line, major peak at rv = 10.7 mL ≈ 258 kDa) or NaCl 1 M (black line, major peaks at rv = 10.7 mL ≈ 258 kDa and rv= 13.7 mL ≈ 68 kDa), or in buffer MES pH 6.5, NaCl 0.5 M (dot grey line rv = 12,6 ≈ 118 kDa). Residues participating in the formation of the additional salt bridge between dimers in G6PDH from **B)** *T. cruzi* and **C)** *C. fasciculata*. In *Cf*G6PDH, an Asparagine residue (N325) substitutes the otherwise conserved Arginine (R323 in *Tc*G6PDH) present in G6PDH from trypanosomatids, hence precluding the formation of a double salt bridge with the highly conserved D334 and E335 (D332 and E333 in *Tc*G6PDH) from a vicinal subunit. Nonetheless, the contiguous R331 of *Cf*G6PDH is yet at a distance suitable to establish an ionic interaction with D334.

Figure 6. Structural NADP$^+$ binding site and catalytic elements connected to Arg323 of *Tc*G6PDH. A) Region involved in binding allosteric NADP$^+$ in human G6PDH (PDB 1QKI; chain A, backbone and ligand shown in magenta) [29,33]. Superimposed is shown the backbone structure of the chain A (red) and chain D (blue) from Δ37N-*Tc*G6PDH. The residues that participate in NADP$^+$ binding in *Hs*G6PDH (K366, R487 and Y503) and are not conserved in *Tc*G6PDH (L409, C528 and T544) are depicted as sticks colored according to the respective backbones. Polar and π interactions are shown with grey and yellow dashed lines, respectively. The Cys528-Cys552 disulfide and the Cys528 sulfenic seen in the crystal structure of Δ37N-*Tc*G6PDH (PDB 6D24) are shown as sticks. **B)** Surface representation of *Tc*G6PDH (PDB 6D24, chain A) with backbone elements of the segment Glu285-Arg323

displayed as green cartoon. Residues key for interaction with G6P (D304 and E285) and catalysis (H309) are shown as sticks. Arg323 and the corresponding negatively charged residues from chain B involved in electrostatic interactions (D332 and E333, blue sticks) are also shown.

Figure 7. Cysteines from the N-terminal extension are responsible for the formation of inter-subunit disulfides in *Tc*G6PDH$_L$. A) SDS-15% PAGE for full-length wildtype (WT) and Arg323Gly (R323G), and ∆37N- (∆37N) *Tc*G6PDH run in the presence (+) or absence (-) of reducing agent (β-mercaptoethanol). **B)** Western blot of C8S, C34S and the double mutant C8S/C34S (C8/34S) of *Tc*G6PDH$_L$ that were pre-reduced with 150 µM DTT (DTT) and, upon removal of excess reducing agent, further treated with 150 µM glutathione disulfide (GSSG) for 45 min or that underwent spontaneous oxidation upon storage for one week in the absence of a reducing agent (spont. oxidation,). The protein samples (300 ng protein/lane) were separated on SDS-12% PAGE under non-reducing conditions. The samples corresponding to the GSSG treatment were separated in a second gel due to lanes constraint.
The bands corresponding to monomeric and dimeric species are indicated with arrows and asterisk, respectively, while the region corresponding to covalent multimeric species is marked with a vertical line. The arrow head denotes a non-specific protein band migrating close above than dimeric *Tc*G6PDH that proved unreactive in Western blot analysis with anti-*Tc*G6PDH serum.

Figure 8. Dynamic of the N-terminal region and cysteine triad of *Tc*G6PDH. Cartoon representation of the N-terminal segment of Δ37N-*Tc*G6PDH (V52-K84) (deep olive color; chain D, PDB 6D24) and Δ57N-*Tc*G6PDH (P62-K84: blue color; chain A, PDB 5AQ1) with bound G6P and NADPH. Substrates (G6P and NADPH), residues involved in substrate binding (L80, K83 and K84) [19] and N-terminal cysteine triad (C53, C94 and C135; highlighted with asterisk for Δ57N-*Tc*G6PDH) are shown as sticks (cyan: carbon, red: oxygen, blue: nitrogen and orange: phosphate, yellow: sulfur).

Figure 9. Catalytic model of *Tc*G6PDH and conformational changes in elements and residues from N-terminal domain involved in ligand binding. A) Superimposition of the protein backbone corresponding to the catalytic (yellow cartoon) [18] and crystallographic (blue cartoon; chain A, PDB 5AQ1) [28] model of *Tc*G6PDH with bound ligands (G6P and $NADP^+$ for the catalytic model, and G6P and NADPH for the crystal structure). The secondary structure elements displaying shifts in their conformation are labeled (i.e. α2, 3, 4, 5 and 6, and β1 and 2). G6P and $NADP^+$(H) are shown as sticks with carbon atoms colored according to the backbone color selected for each structure. Residues important for G6P binding (green lines: interacting with the sugar moiety, and red lines: interacting with the phosphate groups) and shaping the catalytic site (yellow or blue, for the corresponding structures) are shown for **B)** the molecular dynamics model of the ternary enzyme-substrates complex and **C)** the crystal structure of the enzyme-G6P-NADPH complex (chain A, PDB 5AQ1). For both models, the segment connecting β6 with α9 is shown as cartoon (dark grey).

Supplemental information

Figure Legends

Figure S1. Multiple sequence alignment of G6PDH from Kinetoplastid parasites lacking conserved R323. Amino acid sequence alignment for putative G6PDH from *Leptomona seymouri* (Ls), *Leptomona pyrrhocoris* (Lp), *Crithidia fasciculata* (Cf), *Leishmania enrietti* (Le), and of characterized G6PDH from *T. cruzi* (Tc) and *Homo sapiens* (Hs). Strictly conserved or highly similar residues are shown on black background. Residues that in human G6PDH anchor the allosteric $NADP^+$ are highlighted in blue with those not conserved in the *T. cruzi* enzyme marked with yellow. Residues that in *T. cruzi* G6PDH form salt bridges that stabilize the tetramer are highlighted in green. The polar residues of G6PDH from non-pathogenics Kinetoplastids that substitutes the otherwise conserved R323 are highlighted with a yellow frame whereas the non-conserved Arginine of Kinetoplastid G6PDH (R331 in *Cf*G6PDH) that may establish a salt bridge with a strictly conserved Glutamate residue (D334 in *Cf*G6PDH or D332 in *Tc*G6PDH) is framed in red.

Figure S2. Size exclusion chromatography analysis of recombinant *Hs*G6PDH. *Hs*G6PDH (30 uM) was gel filtrated on a Superdex G200 resin (10/300 column) pre-equilibrated in reaction buffer (Tris 50 mM, pH 7.8, NaCl 0.5 M). The major protein peaks shows retention volumes (rv) that correspond to high molecular weight multimers (rv > 8 ml, exclusion volume, > 669 kDa), a tetrameric (rv = 10.2 mL, ≈ 322 kDa, $\alpha 4$) and dimeric (rv = 12.1 mL, ≈138 kDa, $\alpha 2$) species. The peak indicated with an arrow correspond to a contaminant protein of about 45 kDa. The arrowheads at the top of the chromatogram indicate the position of the peaks corresponding to the molecular weight standards separated under the same conditions.

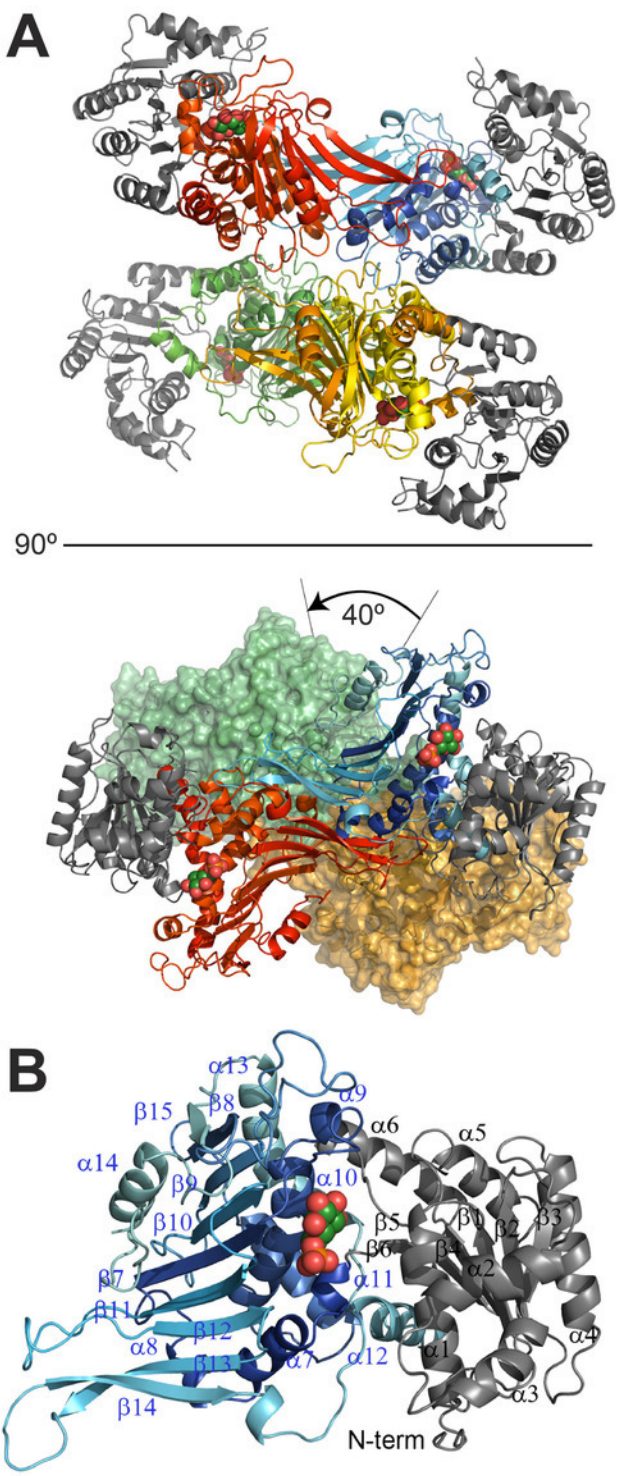
A
90°
40°
B
α13
β15
β8
α9
α6
α5
α14
β9
α10
β10
β5
β1
β2
β3
β6
β4
α2
β7
α11
β11
β12
α8
β13
α7
α12
α1
α4
α3
β14
N-term

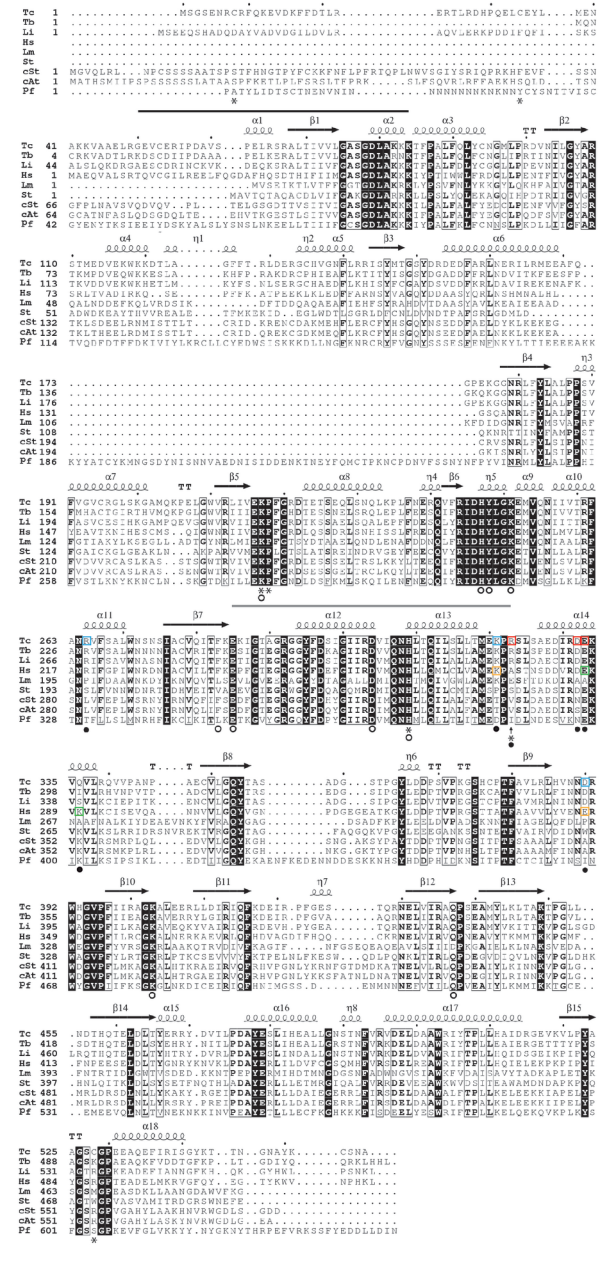

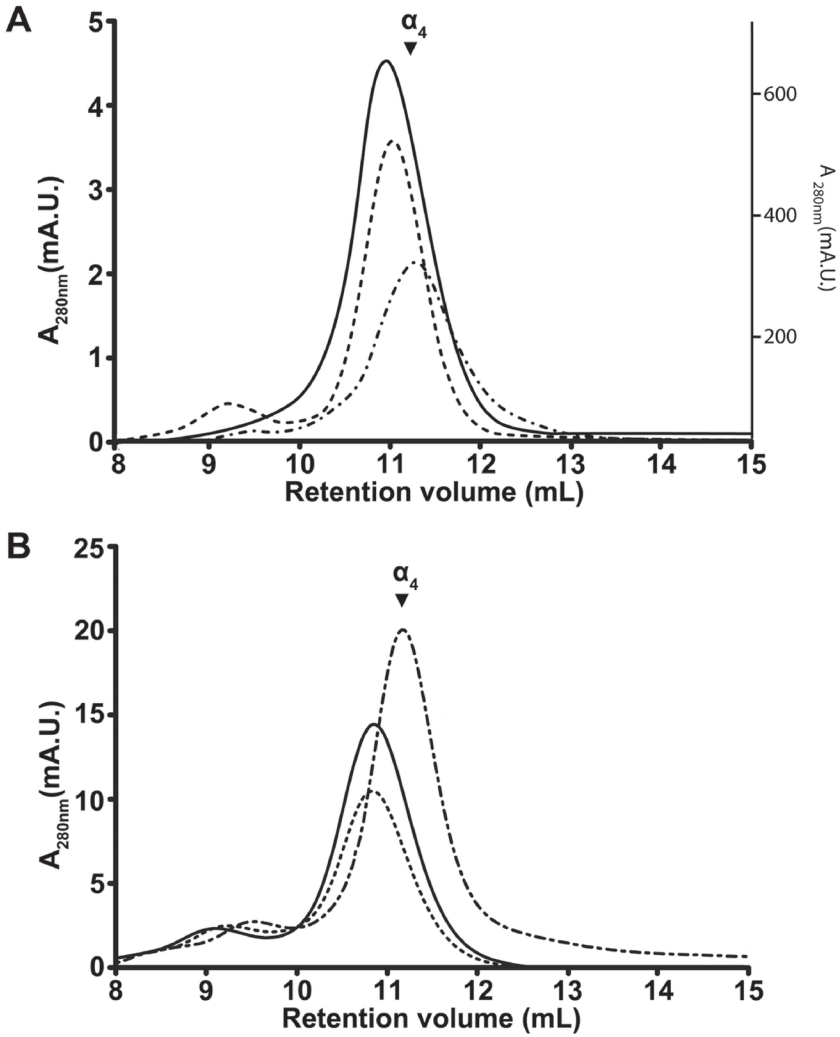
A
α4
A280nm(mA.U.)
A 280nm(mA.U.)
Retention volume (mL)
B
α4
A280nm(mA.U.)
Retention volume (mL)

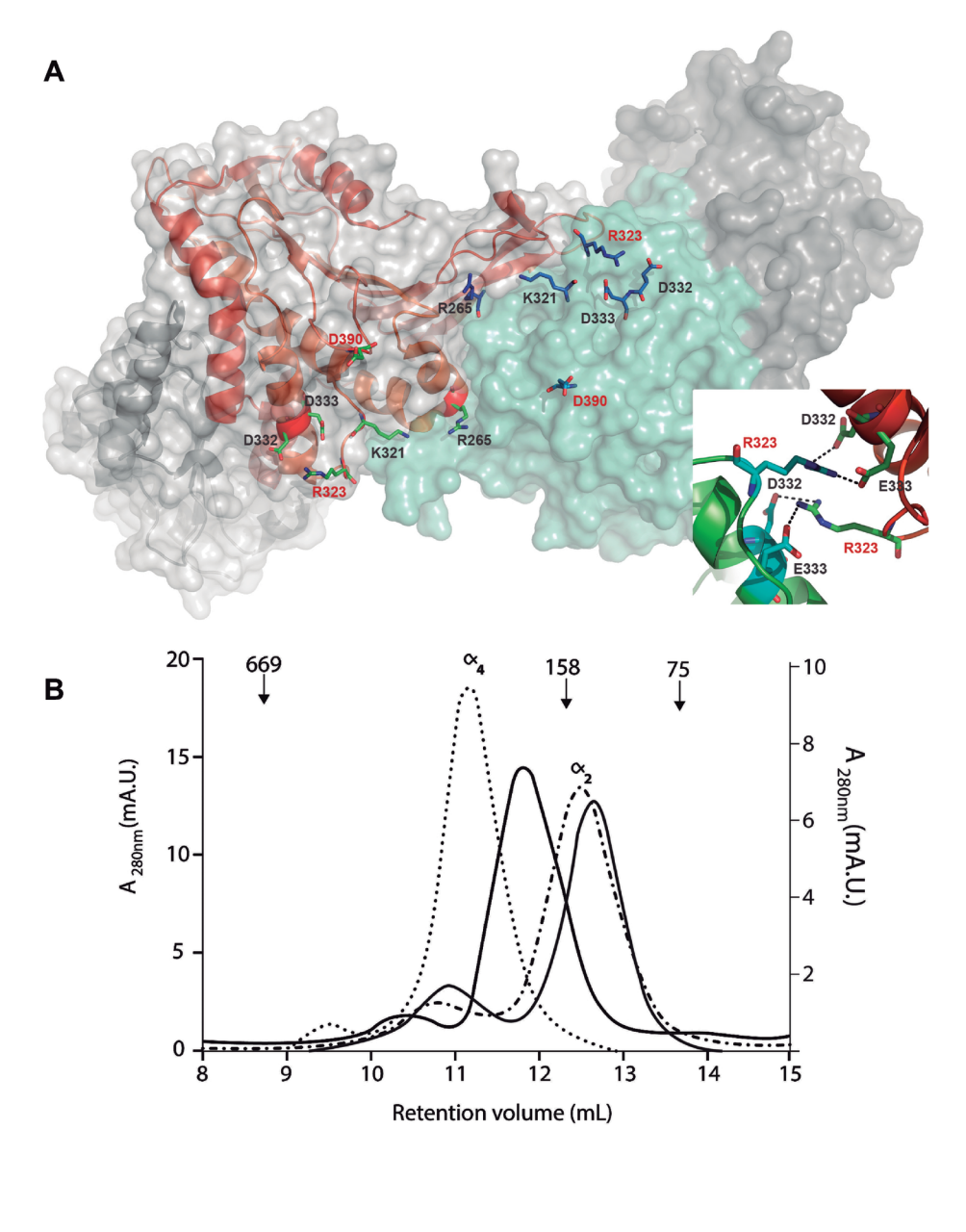
A
R323
K321
D332
D333
R265
D390
D390
D333
D332
K321
R265
R323
D332
R323
D332
E333
R323
E333
B
669
α4
158
75
α2
A 280nm (mA.U.)
A 280nm (mA.U.)
Retention volume (mL)

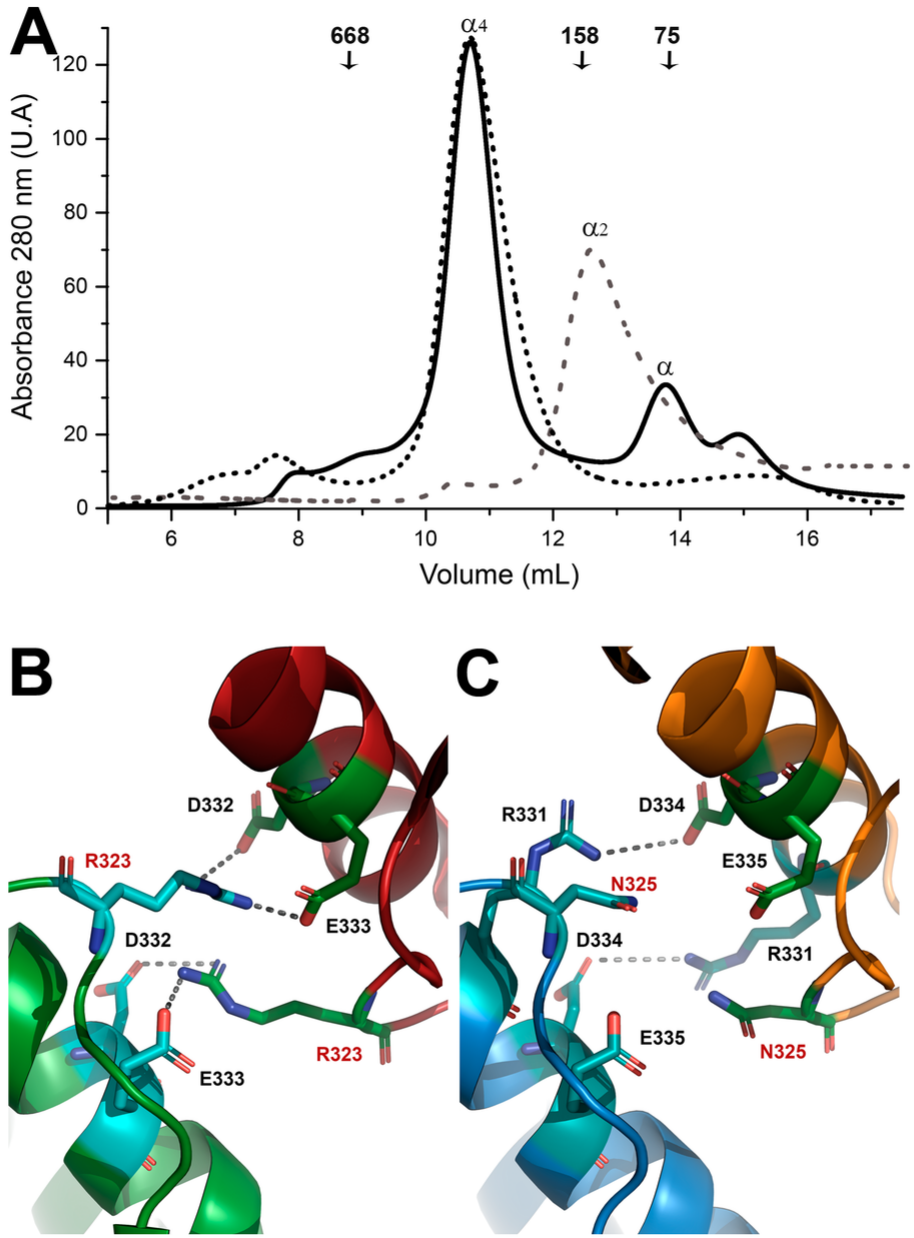
A
668
α4
158
75
α2
α
Absorbance 280 nm (U.A)
Volume (mL)
B
D332
R323
E333
D332
R323
E333
C
R331
D334
N325
E335
D334
R331
E335
N325

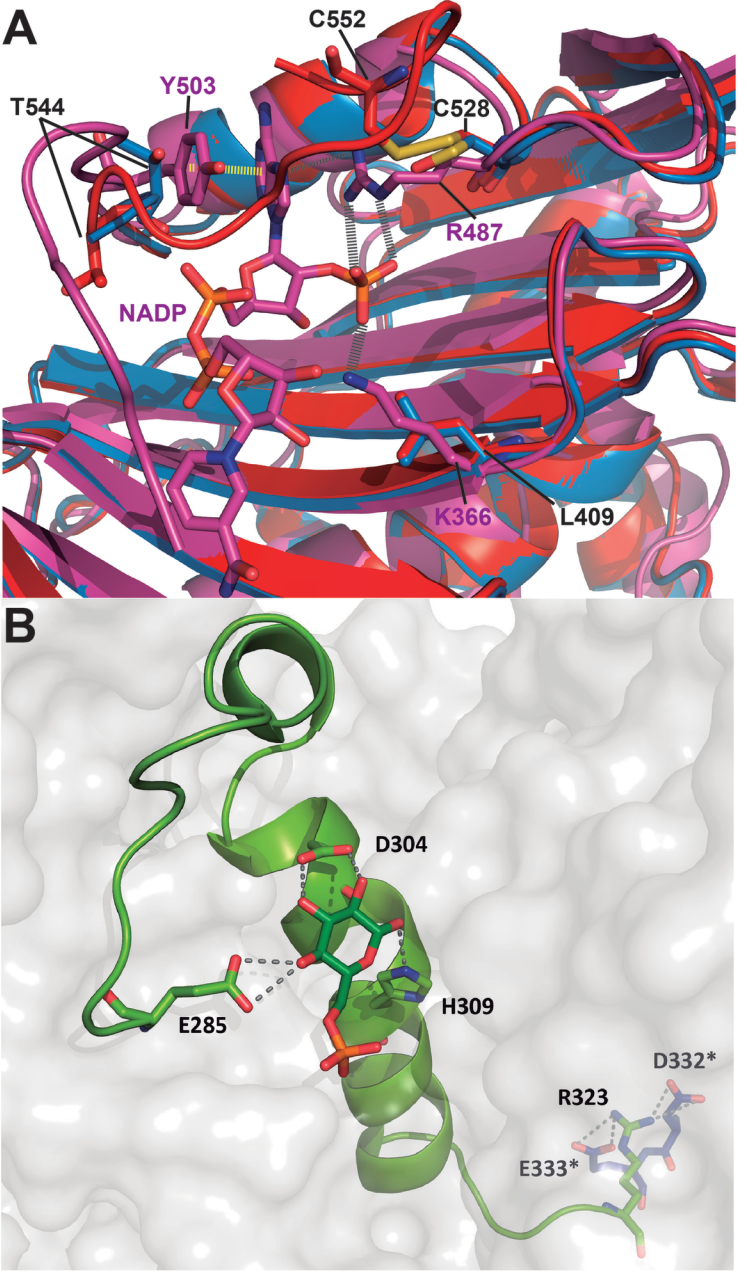
A
C552
Y503
T544
C528
R487
NADP
K366
L409
B
D304
E285
H309
D332*
R323
E333*

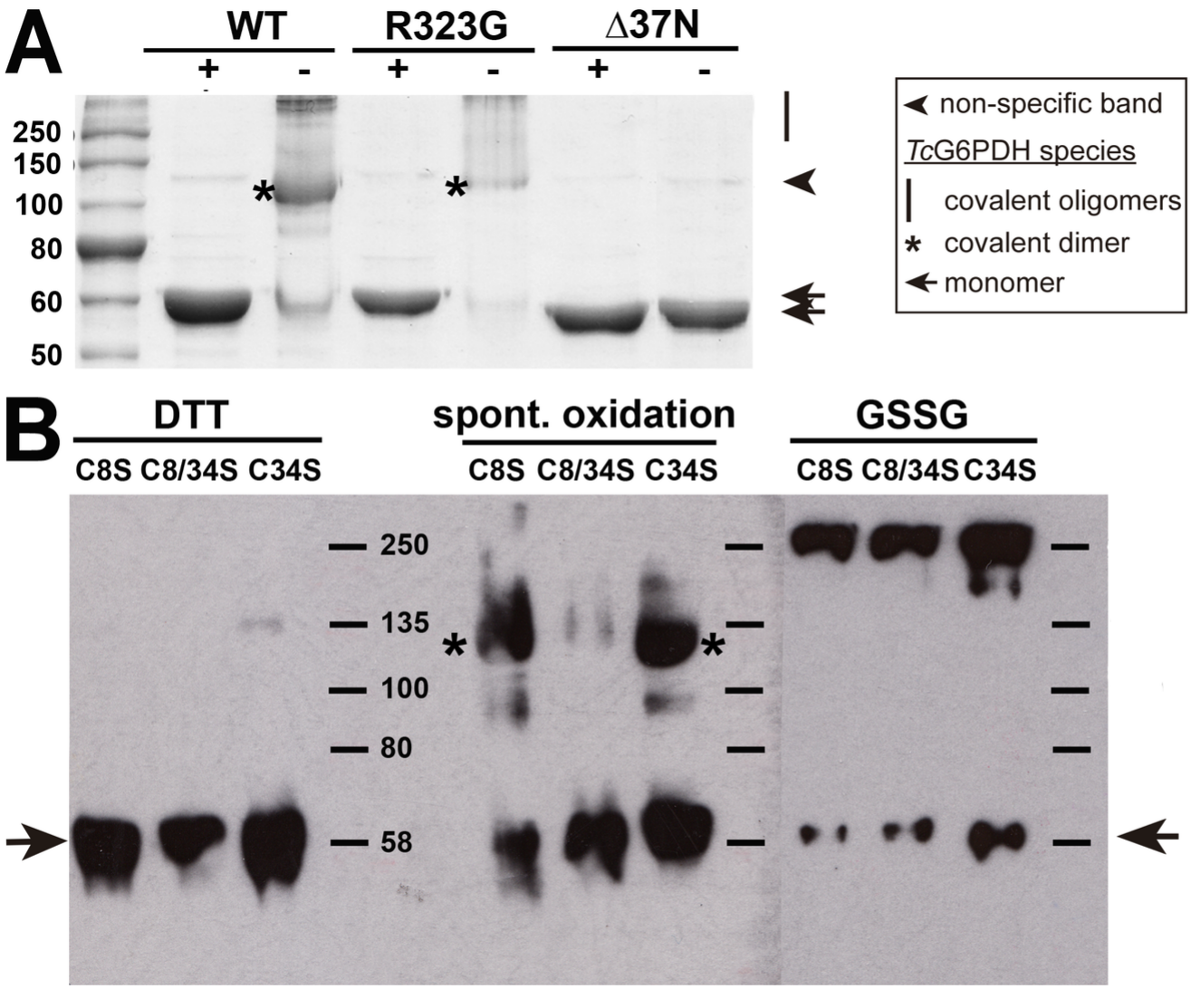
A
WT
R323G
Δ37N
+
-
+
-
+
-
250
150
100
80
60
50
*
*
non-specific band
TcG6PDH species
covalent oligomers
covalent dimer
monomer
B
DTT
spont. oxidation
GSSG
C8S C8/34S C34S
C8S C8/34S C34S
C8S C8/34S C34S
250
135
100
80
58
*
*

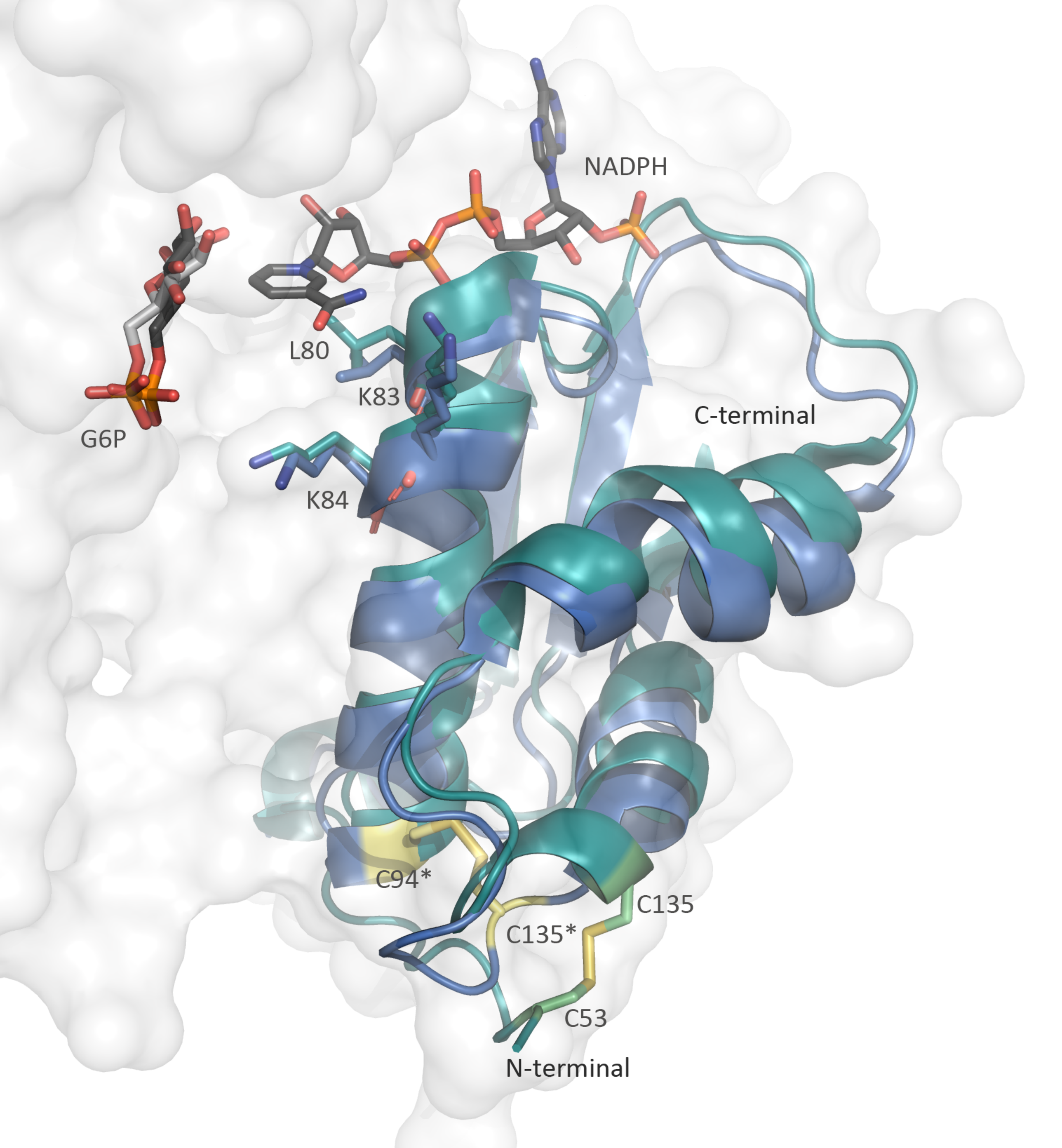
NADPH
L80
K83
K84
G6P
C-terminal
C94*
C135
C135*
C53
N-terminal

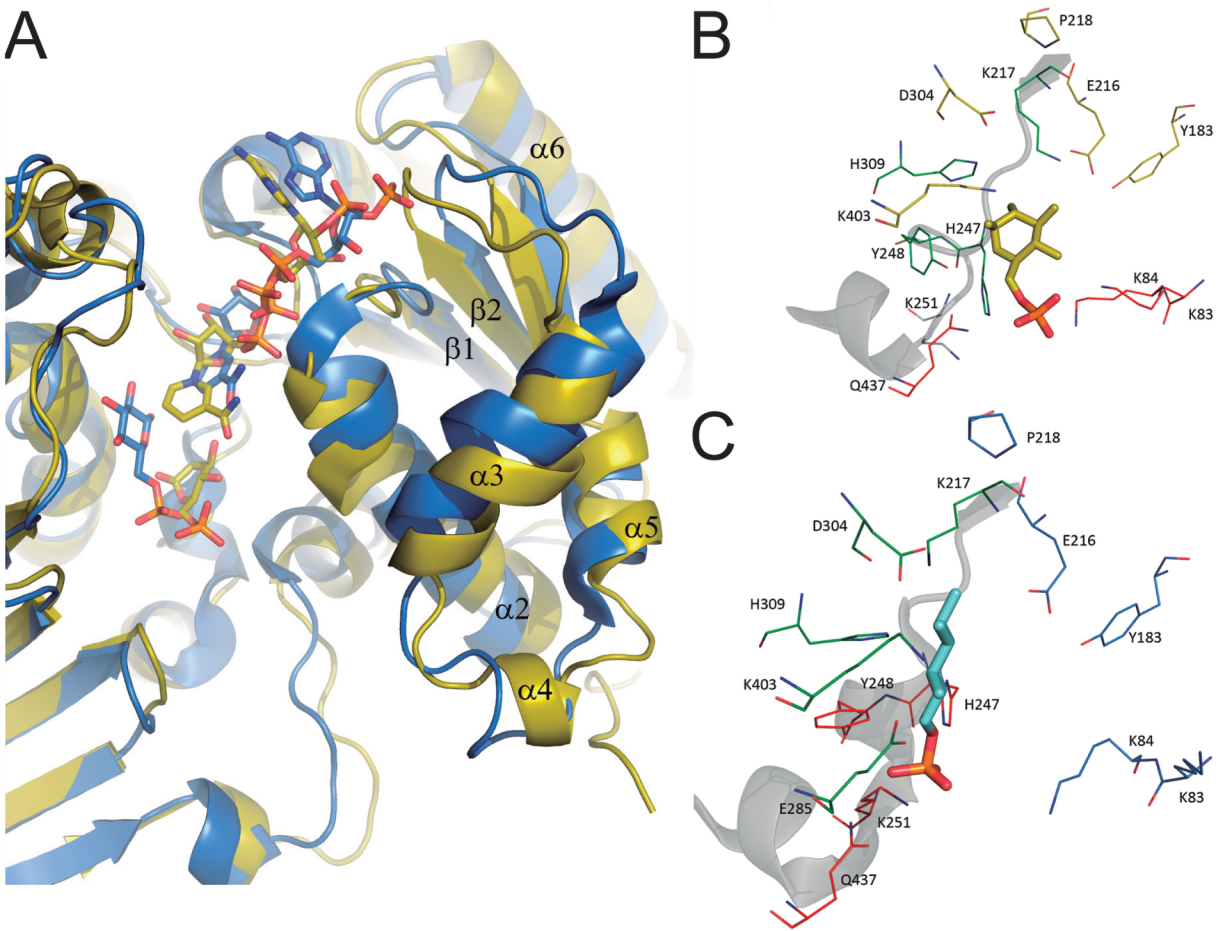
A
α6
β2
β1
α3
α5
α2
α4
B
P218
K217
D304
E216
Y183
H309
K403
H247
Y248
K84
K251
K83
Q437
C
P218
K217
D304
E216
H309
Y183
K403
Y248
H247
K84
E285
K251
K83
Q437

Trypanosoma cruzi G6PDH is a highly stable and redox-regulated tetramer